The NCEP Climate Forecast System

S. Saha[*], S. Nadiga[*], C. Thiaw[*], J. Wang[*], W. Wang[**], Q. Zhang[**],
H. M. van den Dool[**], H.-L. Pan[*], S. Moorthi[*], D. Behringer[*], D. Stokes[*],
G. White[*], S. Lord[*], W. Ebisuzaki[**], P. Peng[**], P. Xie[**]

Submitted to the J. Climate

[*]Environmental Modeling Center
National Centers for Environmental Prediction
NWS/NOAA/DOC, Washington, D. C.

[**]Climate Prediction Center
National Centers for Environmental Prediction
NWS/NOAA/DOC, Washington, D. C.

Corresponding author address :
Dr. Suranjana Saha, Environmental Modeling Center,
5200 Auth Road, Camp Springs, MD 20746.
E-mail : Suranjana.Saha@noaa.gov

Abstract

The Climate Forecast System (CFS), the fully coupled ocean-land-atmosphere dynamical seasonal prediction system that became operational at NCEP in August 2004, is described and evaluated in this paper. The CFS provides important advances in operational seasonal prediction on a number of fronts. For the first time in the history of U.S. operational seasonal prediction, a dynamical modeling system has demonstrated a level of skill in forecasting U.S. surface temperature and precipitation that is comparable to the skill of the statistical methods used by the NCEP Climate Prediction Center (CPC). This represents a significant improvement over the previous dynamical modeling system used at NCEP. Furthermore, the skill provided by the CFS spatially and temporally complements the skill provided by the statistical tools. The availability of a dynamical modeling tool with demonstrated skill should result in overall improvement in the operational seasonal forecast products produced by CPC.

The atmospheric component of the CFS is a lower resolution version of the Global Forecast System (GFS) that was the operational global weather prediction model at NCEP during 2003. The ocean component is the GFDL Modular Ocean Model version 3 (MOM3). The previous dynamical seasonal forecast system used at NCEP consisted of the 1998 GFS (a.k.a. MRF) and the GFDL MOM1 ocean model. In addition to the replacement of the oceanic and atmospheric components, there are several important improvements inherent in the new CFS relative to the previous dynamical forecast system. These include: (i) The atmosphere-ocean coupling spans almost all of the globe (as opposed to the tropical Pacific only); (ii) The CFS is a fully coupled modeling system with no flux correction (as opposed to the previous uncoupled 'tier-2' system, which

employed multiple bias and flux corrections); (iii) A set of fully coupled retrospective forecasts covering a 24 year period (1981-2004), with 15 forecasts per calendar month out to nine months into the future, have been produced with the CFS. In contrast "perfect" (i.e., observed) SST was prescribed in the production of the retrospective forecasts for the previously operational dynamical forecast system.

These 24 years of fully coupled retrospective forecasts are of paramount importance to the proper calibration (bias correction) of subsequent operational seasonal forecasts. They provide a meaningful à *priori* estimate of model skill that is critical in determining the utility of the real-time dynamical forecast in the operational framework. The retrospective dataset also provides a wealth of information for researchers to study interactive atmosphere-land-ocean processes.

Outline of the Paper

1. Introduction

It is generally assumed that the memory of the geophysical system that could aid in seasonal climate forecasting resides mainly in the ocean. The strong El Nino events of 1982/83 and 1997/98 appeared to provide empirical evidence that, at least in some cases, this is indeed true (Barnston et al. 1999). It is thus logical for the scientific community to develop global coupled atmosphere-ocean models to aid in seasonal forecasting. At the National Centers for Environmental Prediction (NCEP) in Washington, D. C., coupled ocean-atmosphere models are looked upon as an extension of existing numerical weather prediction infrastructure. For this task, one obviously needs numerical models of both the atmosphere and the ocean, along with their own data assimilation systems. Global numerical prediction models for weather (and their attendant data assimilation systems) have matured since about 1980 and are the tool of choice today for day-to-day global weather forecasting out to one or two weeks. On the other hand, while numerical prediction models for the ocean coupled to an atmosphere have existed for a long time in research mode (Manabe and Bryan 1969), such models had not been tested in real time

forecasting, nor had a data assimilation system been developed for the ocean until the 1990's. Ji et al. (1995) described the early data assimilation effort at NCEP (then NMC) for a tropical strip of the Pacific Ocean using the Modular Ocean Model, version 1(MOM1), developed at the Geophysical Fluid Dynamical Laboratory (GFDL) in Princeton, NJ. An ocean reanalysis was performed by Ji et al. (1995) and Behringer et al. (1998) for the Pacific basin (20°S-20°N) starting from July 1982 onward. This provided the ocean initial conditions for coupled forecast experiments, including retrospective forecasts.

The first coupled forecast model at NCEP in the mid-nineties consisted of an ocean model for the Pacific Ocean, coupled to a coarser resolution version of the then operational NMC Medium Range Forecast (MRF) model. The atmospheric model had a spectral triangular truncation of 40 waves (T40) in the horizontal and 18 sigma levels (L18) in the vertical (Ji et al. 1994, 1998). In order to avoid very large biases, "anomaly flux corrections" were applied at the ocean-atmosphere interface. The final stand alone atmospheric forecasts were made in 'tier-2' mode, in which the sea surface temperature fields produced during the coupled integration were used, after more bias correction, as a prescribed time varying lower boundary condition for an ensemble of Atmospheric General Circulation Model (AGCM) runs. The 'tier-2' approach and its attendant flux correction procedure is common to this day. Since the SST outside the tropical Pacific had to be specified as well, damped persistence became a common substitute. This early set-up of the coupled model was known as MRFb9x for the atmospheric component, and CMP12/14 for the oceanic component. The atmospheric component was upgraded both in physics and resolution to T62L28 several years later (Kanamitsu et al. 2002B).

This upgraded system, known as the Seasonal Forecast Model (SFM) was operational at NCEP until August 2004.

Very few operational centers have been able to afford the development of a coupled atmosphere-ocean-land model for real time seasonal prediction. The European Centre for Medium-Range Weather Forecasts (ECMWF) has been engaged in this effort along with NCEP. At ECMWF, the first coupled model (System-1) was developed around 1996 (Stockdale et al. 1998), with a second update (System-2) in 2003 (Anderson et al. 2003). An evaluation against empirical models can be found in Van Oldenborgh et al. (2005). In Europe, a large experiment is underway, called the Development of a European Multimodel Ensemble system for seasonal to interannual prediction (DEMETER), in which six different atmospheric models are coupled to the same ocean model as described in Palmer et al (2005). At most other centers, such as the International Research Institute for Climate Prediction (IRI), the 'tier-2' system continues to be used (Barnston et al. 2003).

The purpose of this paper is to document the new NCEP Climate Forecast System (CFS), which became operational in August 2004. As part of the design of the CFS, three major improvements were made to the old operational coupled forecast system. First, the component models have been greatly modernized. The ocean model, MOM1, has been replaced by MOM3, and the atmospheric model, SFM, has been replaced by a coarse resolution version of the operational (as of 2003) NCEP Global Forecast System (GFS). Most notably, this change includes an upgrade in vertical resolution from the old SFM, from 28 to 64 sigma layers. Second, the ocean-atmosphere coupling is now nearly global (64°N-74°S), instead of only in the tropical Pacific Ocean, and flux correction is

no longer applied. Thus, the CFS is a fully 'tier-1' forecast system. The coupling over the global ocean required an important upgrade in the ocean data assimilation as well (see Behringer et al. 2005). Third, an extensive set of retrospective forecasts ('hindcasts') was generated to cover a 24 years period (1981-2004), in order to obtain a history of the model. This history can be used operationally to calibrate and assess the skill of the real-time forecasts. Hindcast histories that were generated to assess the skill of all previous tier-2 seasonal forecast systems in use at NCEP were obtained by prescribing 'perfect' (observed) SST. This methodology is often assumed to provide an 'upper limit of predictability.' However, this method did not provide an accurate estimate of the skill of the tier-2 operational model, which used predicted, not 'perfect' SST. This methodology is still being practiced elsewhere to determine the 'skill' of multi model ensembles, etc. In the current CFS system, the model skill is assessed solely by the use of a tier-1 retrospective set of forecasts.

The first two items include several advances in physics and a much better coupled system, both in multi-decadal free runs (Wang et al. 2005) and in nine month forecasts from many initial conditions. Specifically, the ENSO simulation and the synoptic tropical activity (Madden Julian Oscillations, easterly waves, etc.) appear state of the art in the CFS with 64 vertical levels. The third item, while costly in terms of computer time and resources, is especially important to the user of the model in that a robust measure of skill is provided.

The lay-out of the paper is as follows: In sections 2 and 3 we describe the components of the CFS and the organization of the hindcasts respectively. In section 4 we discuss the CFS performance for its main application as a monthly/seasonal forecast

tool. In section 5 we present some diagnostics highlighting strengths and systematic errors in the CFS. Summary and conclusions are found in Section 6.

2. Overview of the Climate Forecast System

The atmospheric component of the CFS is the NCEP atmospheric GFS model, as of February 2003 (Moorthi et al. 2001). Except for having a coarser horizontal resolution, it is the same as that used for operational weather forecasting with no tuning for climate applications. It adopts a spectral triangular truncation of 62 waves (T62) in the horizontal (equivalent to nearly a 200 Km Gaussian grid) and a finite differencing in the vertical with 64 sigma layers. The model top is at 0.2 hPa. This version of the GFS has been modified from the version of the NCEP model used for the NCEP/NCAR Reanalysis (Kalnay et al. 1996 ; Kistler et al. 2001), with upgrades in the parameterization of solar radiation transfer (Hou, 1996 and Hou et al. 2002), boundary layer vertical diffusion (Hong and Pan 1996), cumulus convection (Hong and Pan 1998), gravity wave drag (Kim and Arakawa 1995). In addition, the cloud condensate is a prognostic quantity with a simple cloud microphysics parameterization (Zhao and Carr 1997, Sundqvist et al. 1989, Moorthi et al. 2001). The fractional cloud cover used for radiation is diagnostically determined by the predicted cloud condensate.

The oceanic component is the GFDL Modular Ocean Model V.3 (MOM3) (Pacanowski and Griffies 1998), which is a finite difference version of the ocean primitive equations under the assumptions of Boussinesq and hydrostatic approximations. It uses spherical coordinates in the horizontal with a staggered Arakawa B grid and the z-coordinate in the vertical. The ocean surface boundary is computed as an explicit free

surface. The domain is quasi-global extending from 74°S to 64°N. The zonal resolution is 1°. The meridional resolution is 1/3° between 10°S and 10°N, gradually increasing through the tropics until becoming fixed at 1° poleward of 30°S and 30°N. There are 40 layers in the vertical with 27 layers in the upper 400 m, and the bottom depth is around 4.5 Km. The vertical resolution is 10 m from the surface to the 240-m depth, gradually increasing to about 511 m in the bottom layer. Vertical mixing follows the non-local K-profile parameterization of Large et al. (1994). The horizontal mixing of tracers uses the isoneutral method pioneered by Gent and McWilliams (1990) (see also Griffies et al. 1998). The horizontal mixing of momentum uses the nonlinear scheme of Smagorinsky (1963).

The atmospheric and oceanic components are coupled with no flux adjustment or correction. The two components exchange daily averaged quantities, such as heat and momentum fluxes, once a day. Because of the difference in latitudinal domain, full interaction between atmospheric and oceanic components is confined to 65°S to 50°N. Poleward of 74°S and 64°N, SSTs needed for the atmospheric model are taken from observed climatology. Between 74°S and 65°S, and between 64°N and 50°N, SSTs for the atmospheric component are weighted average of the observed climatology and the SST from the ocean component of the CFS. The weights vary linearly with latitude, such that the SSTs at 74°S and 64°N equal observed climatology and the SSTs from 65°S and 50°N equal values from the ocean component. Sea ice extent is prescribed from the observed climatology.

The ocean initial conditions were obtained from the Global Ocean Data Assimilating System (GODAS) (Behringer, et al. 2005), which was made operational at NCEP in

September 2003. The ocean model used in GODAS is the same as used in the CFS retrospective forecasts. The ocean data assimilation system uses the 3-D variational technique of Derber and Rosati (1989), modified to include vertical variations in the error covariances (Behringer et al., 1998). The ocean model in GODAS was forced with weekly fluxes of heat (Q), surface buoyancy fluxes (E-P) and wind stress vectors (τ) from NCEP Reanalysis-2 (Kanamitsu et al. 2002A). Also, a relaxation technique (with a relaxation time scale of 90 days) was used to relax the simulated GODAS sea surface temperatures to Reynolds SST (Reynolds and Smith 1994), and the sea surface salinity fields were relaxed to Levitus climatological monthly fields of sea surface salinity (Levitus et al. 1994). The subsurface temperature data that were assimilated were obtained from expendable bathythermographs (XBTs), the tropical atmosphere-ocean (TAO) array of moored buoys, and the ARGO network of floats. As shown in Maes and Behringer (2000) and Ji et al. (2000), the subsurface salinity variability strongly influences the density stratification in the ocean through the formation of salt-stratified barrier layers, especially in the western and central equatorial Pacific Ocean. Therefore, a climatological Temperature-Salinity (T-S) relationship was imposed to correct the subsurface salinity profiles in the model runs.

For the land surface hydrology the two layer model described in Mahrt and Pan(1984) is used here.

3. Design of the CFS Retrospective Forecasts

The CFS includes a comprehensive set of retrospective runs that are used to calibrate and evaluate the skill of its forecasts. Each run is a full nine month integration.

The retrospective period covers all 12 calendar months in the 24 years from 1981 to 2004. Runs are initiated from 15 initial conditions that span each month, amounting to a total of 4320 runs. Since each run is a nine month integration, the CFS was run for an equivalent of 3240 years! Due to limitations in computer time, only 15 days in the month were used as initial conditions. These initial conditions were carefully selected to span the evolution of both the atmosphere and ocean in a continuous fashion.

The atmospheric initial conditions were from the NCEP/DOE Atmospheric Model Intercomparison Project (AMIP) II Reanalysis (R2) data (Kanamitsu et al. 2002A), and the ocean initial conditions were from the NCEP Global Ocean Data Assimilation (GODAS) (Behringer 2005). Each month was partitioned into 3 segments. The first was centered on the pentad ocean initial condition of the 11th of the month, i.e. the 5 atmospheric initial states of 9th, 10th, 11th, 12th and 13th of the month used the same pentad ocean initial condition of the 11th. The second set of 5 atmospheric initial states of 19th, 20th, 21st, 22nd and 23rd of the month used the same pentad ocean initial condition of the 21st of the month. The last set of 5 atmospheric initial states include the second-to-last day of the month, the last day of the month, and 1st, 2nd and 3rd days of the next month used the same pentad ocean initial condition of the 1st of the next month. These 15 runs from the retrospective forecasts form the ensemble that is used by operational forecasters for calibration and skill assessment for the operational monthly seasonal forecast at NCEP. Note that no perturbations of the initial conditions are applied for making the ensemble forecast. The perturbations come automatically by taking atmospheric states one day apart, but this may not be optimal.

A hypothetical example is the official forecast made by the Climate Prediction Center (CPC) of NCEP around the 10th of February. February is then considered to be the month of forecast lead zero, March is the month of forecast lead one, and so on. Runs originating from initial conditions after the 3rd of February from the retrospective forecasts are not considered for calibration of the February forecasts. This is done because in 'operations' there is a 7-day lag in obtaining the ocean initial conditions (see Section 7 that explains the design of operational CFS forecasts). The 15 members in the ensemble thus include 9th - 13th January, 19th - 23rd January, and 30th January - 3rd of February. This method of calibration and subsequent skill assessment is used throughout this paper in order to replicate the operational procedures used at NCEP and to provide the most accurate assessment possible of the CFS skill to the forecasting community.

It is important to note that the CFS model codes were 'frozen' in June 2003. The running of the entire retrospective forecasts and operational implementation of the CFS that took nearly a year, were made with these codes. No changes or tuning for results were made to these codes during the execution of the forecasts. These forecasts truly represent the "history" of the operational CFS.

4. CFS Performance Statistics

In this section we review the performance of CFS retrospective forecasts, mainly in terms of skill as measured by the anomaly correlation (AC) against observations. We refer to the Appendix 1 for details about definitions, and the adjustments necessary in using the AC in the context of (i) systematic error correction and (ii) cross-validation, which has been adhered to in computing the results that are presented in this paper. In

this section we correct for the overall mean error by subtracting the model climatology from model forecasts. See details in Appendix.

We focus on , in order, the prediction of SST in the Nino3.4 area (5S-5N;170W-120W) of the tropical Pacific, SST in mid-latitudes, surface air temperature, precipitation, 500 hPa geopotential and soil moisture. In all cases we verify either monthly or seasonal mean values. In most cases we verify the bias corrected ensemble mean averaged over the 15 ensemble members. In some cases, we also compare to other tools : either a previous model or some statistical tools that are being used by CPC. When we quote scores for 1981-2003 this includes verifying data well into 2004 for the longer lead forecasts starting in 2003.

Fig 1 shows the skill (anomaly correlation) of the Nino3.4 SST forecasts over the period 1981-2003. Nino3.4 SST is probably the single most predictable entity. We use here, and in many graphs below, a display of forecast lead in months (on the Y-axis) versus the target or verification month (on the X-axis). Forecasts for December and January exceed 0.9 in correlation for leads out to 5 months, i.e. these forecasts were initiated during the previous summer. However, forecasts for the Northern Hemisphere summer months, most notably for July, are more difficult, with correlations as low as 0.4 at leads of 7 months. The sudden drop in skill near April is known as the spring barrier. A display of forecast lead versus initial month (not shown) shows a "return of skill", because the decay of skill with lead time is interfered with by a strong seasonality of the errors.

CPC has maintained an archive of Nino3.4 SST predictions ***in real time***. Fig. 2 shows the overall scores as a function of forecast lead for seasonal Nino3.4 SST

prediction by various methods from 1997 to the present. The correlations shown are evaluated on all cases in the period. The CFS, the only retrospective method in this display, is shown by red bars. The other methods are NCEPs previous coupled model and labeled CMP14, the Canonical Correlation Analysis (CCA) (Barnston and Ropelewski 1992), Constructed Analogue (CA) (Van den Dool 1994), the 'Markov' method (Xue et al. 2000) and a Consolidation (CON) of all methods available in real time (Unger et al. 1996). The CFS results, if achieved in real time, would easily have been competitive with all the other methods and, in fact, would have been a big improvement over the CMP14. The main reason CON did worse than the best single method is that CMP14 scored much lower over 1997 onward than anticipated, based on its 1982-96 evaluation. This illustrates the importance of an evaluation that will hold up on independent data.

Fig 3 is the same as Fig 1, except that the ensemble mean over 14 members is verified against the one member left out. This procedure measures potential predictability under perfect model assumptions. Although scores for Nino3.4 SST are already very high, there is a suggestion of large improvements still ahead, especially in summer.

Ever since Barnston et al. (1994), the standard has been the performance of Nino 3.4 SST prediction at a lead of 6 months. As an example, for initial conditions in April, Fig.4 shows, as a time series, the observations and forecasts (by CFS, CMP-14 and CA) for the following November. Relative to Fig.2 we note that the CFS not only has an overall high correlation, but also maintains amplitude in the forecast better than the other methods .

In Figs 1-3 the variable to be verified was averaged in space to be consistent with the Nino34 'index'. Below we report traditional skill estimates as per anomaly

correlations, without any space averaging. Keep in mind that scores for the Nino34 area would drop by 0.05 to 0.1 or so if the space averaging is not applied.

The CFS is the first NCEP coupled model for the near global oceans. While the main skill continues to be in the tropical Pacific, we can now begin to evaluate where we stand, for instance, in the prediction of mid-latitudes SST. Although much less than Nino3.4, Fig. 5 shows appreciable skill in SST forecasts for most target months at short leads in the NH, an area defined as all ocean grid points north of 35°N (no spatial mean). At longer leads, the skill in the NH pales in comparison to Nino3.4, and only February and March have a slight measure of skill out to a few months. We speculate this may well be due to mid-latitude atmospheric teleconnection patterns related to the tropics, strongest in February, leaving a mark on the mid-latitude oceans.

Fig. 6 is as Fig 5, but now showing the potential predictability of mid-latitude SST. Improvement is seen (and can be expected under perfect model assumptions) for many leads, but fundamentally the mid-latitudes appear less predictable than the tropical Pacific.

The SST forecasts, except for some marine interests, are not in, and of themselves, of great practical importance. We now move to weather elements over land, as well as 500hPa geopotential (Z500) and soil moisture as an aid in interpreting the practical skill of the CFS. Fig.7 shows the skill of monthly mean (ensemble mean) surface air temperature at 2 meters above ground (T2m) and precipitation (P) over the extratropical NH land north of 22.5N. Already at lead 1, these skills are extremely low, and only in summer for T2m, and winter for precipitation, is there a suggestion of non-

zero correlation (for all grid points combined). These numbers obviously improve a little when 3-month means are used or specific regions are considered (not shown).

Fig. 8 shows similar displays of skill for monthly mean 500mb height and soil moisture in the upper 2 meter soil. Skill for 500mb height is quite low in NH extratropics, and only worth mentioning in the NH winter months. Notice also the significant error bars on correlations which are very low for a field with few degrees of freedom, resulting in a noisy picture.

Fig. 8 also shows very high skill for soil wetness. While this skill relates mainly to high persistence, it nevertheless conveys information about the initial condition to the lower atmosphere which is known several months ahead of time. It appears that the summer skill in T2m is caused by soil wetness, while the winter skill in P is consistent with the skill in circulation (Z500). The words 'coupled model' should be thought of as including the coupling to the soil also. Potential predictability estimates (not shown) confirm the idea of skill for P in winter and T2m in summer, although we cannot report anything above 0.35 (domain averaged) in correlation, thus suggesting a low predictability ceiling.

Figs. 9 and 10 show the spatial distribution of the anomaly correlation at lead 1 month of the seasonal mean for T2m (Fig.9) and P (Fig.10) over the United States, averaged over June, July and August (JJA) on the left and December, January and February (DJF) on the right respectively. Local correlations less than 0.3, deemed insignificant in CPC operation, are not contoured. In JJA, the skill is restricted to the Northwest for both P and T2m, while most of the country has no demonstrable skill. In DJF, the skill is better, and situated mainly across the south for P, and in weaker form

across both the north and the south for T2m. The DJF picture of skill would be consistent with ENSO composites, i.e. mainly from years like 1982/83 and 1997/98. Skill for P in Florida in DJF is exceedingly high. Fig. 9 and 10 also address the issue of ensemble size. From top to bottom they show the usage of 5, 10, and 15 members for making the ensemble mean, respectively. Although the pattern should stabilize more for 15 members, one can observe that, leaving details aside, the 5 member ensemble has a similar distribution of skill in space. This is a demonstration that the CFS has reasonably stable skill.

Figs.11 and 12 are similar to Figs. 9 and 10, except that we now compare the 15-member ensemble mean (left column) to one of CPC's control statistics, the CCA (Barnston 1994) in the right column. The comparison is only coarse, since CCA is available for a much longer period (1942-2002). Fig. 11 is for lead 1 seasonal T2m and Fig. 12 is for seasonal P forecasts for the four 'official' seasons of March-April-May (MAM), June-July-August (JJA), September-October-November (SON) and December-January-February (DJF). We now face these questions: Does the CFS have skill ? And if so, does it (or CCA for that matter) add any skill over and above what we know already from other methods ? The latter is a subtle (difficult) issue when skill is low and especially when there are many methods. In Figs. 11 and 12 it is encouraging that CFS and CCA skill do not always occur at the same geographical location, i.e. they appear complementary. Even when identical skill occurs at the same spot there is a possibility that the skillful forecasts happen in different years due to different predictor information being exploited, such that a combination of CCA and CFS may score higher. If the source of skill is the same (and it often is) it will be hard to improve upon a single tool. This

topic of consolidation (Van den Dool and Rukhovets 1994 ; Peng et al. 2002) will be the subject of future studies. On the first question (does CFS have skill?), Figures like Figs 11 and 12 should aid the CPC forecasters. In areas left blank there is no skill. In areas of correlation >=0.3 there is evidence of skill in proportion to the correlation.

The situations most relevant to society are 'extremes', and so we close this section with a few comments about skill of the forecasts when extremes were observed (Saha 2004). We define extreme here as anomaly larger than 2 standard deviations. We then calculate the anomaly correlation over this small sample of cases (extremes of either sign). Fig. 13 shows the skill as a function of lead and target month when a monthly T2m extreme was observed in one of the four quadrants of the US (defined by 100°W and 40°N). Fig.14 is the same, but now for P. There is some skill, with correlations numerically higher than in Fig. 7, but noisier because the sample is smaller. Skill in T2m extremes is mainly in summer, while skill in P resides mainly in winter, in rough agreement with full sample results in Fig.7. This analysis is not complete. A more complete study of extremes is needed, including analysis and verification of cases where the model forecasts an extreme.

5. CFS Diagnostics

In this section we present assorted analyses of model behavior and errors. The emphasis here is on physical interpretation and a route to possible model improvements.

(a) Model Climate Drift

The model climate drift refers to the evolution with forecast lead time of the deviation of model climatology from observed climatology. Here the climatology for a

specific season is defined as the average of the seasonal means over the retrospective period (1982-2004). For the model, the seasonal means are from the retrospective forecasts for that season. For observations, the SST is from the optimally interpolated (OI) SST dataset (Reynolds et al, 2002), the precipitation is from the CPC Merged Analysis of Precipitation (CMAP) Xie-Arkin dataset (Xie and Arkin 1997), and the 200hPa height is from the Reanalysis-2 (Kanamitsu et al. 2002A). (In general we use GODAS for verification and validation, but in section 5(a) the OI-SST is used in favor of GODAS' sea-water temperature at 5 meter depth.)

Fig. 15 exhibits the model climate drift in SST for DJF and JJA seasons and for 3-month lead and 6-month lead retrospective forecasts respectively. It is evident that the bias for the DJF season and 3-month lead (see panel 15b) is quite modest. In most areas of the global oceans it is less than 0.5^{o}C. Stronger bias occurs only in the small areas of the eastern equatorial Pacific and equatorial Atlantic and along the coasts (particularly the west coasts) of major continents in middle and higher latitudes. For the 6-month lead retrospective forecasts (see panel 15c), the bias gets slightly stronger in the tropical Pacific and Indian oceans, indicating the tropical oceans drift away more as lead time increases. For the JJA season, the SST bias in the tropics is comparable to the DJF season, but in middle and higher latitudes, particularly in the northern hemisphere, it is much stronger. Warm biases with magnitude reaching or exceeding 2^{o}C are seen across the North Pacific and North Atlantic in higher latitudes. As lead time increases from 3-month to 6-month (see panel 15e and 15f), the weak cold biases in the middle latitudes of Pacific get stronger, but interestingly, the cold biases in the equatorial Pacific becomes weaker.

Fig. 16 shows the same model climate drift but now for precipitation rate. Evidently the major biases are in the tropics, no matter what season or what forecast lead. For the DJF season (panel 16a and 16b), the biases are characterized by dryness over the equatorial oceans and in the South Pacific Convergence Zone (SPCZ) area, and wetness along the flanks of the dry areas. . This corresponds to a north and eastward shift in the tropical Pacific precipitation. The biases get stronger as the lead time increases, similar to the situation with SST. For the JJA season (panel 16c and 16d), the dryness happens mainly in the western tropical Pacific Ocean and in the eastern Indian Ocean. The wetness patterns are similar to the DJF season, except in the South Atlantic Ocean where the errors in JJA are less

Fig. 17 is for the model climate drift in 200 hPa eddy geopotential. As expected, the major features of the bias are in the extra tropics. For the DJF season (panel 17a and 17b), the positive bias in the western and northwestern Pacific and its downstream wave train-like patterns suggests the geopotential bias in the northern hemisphere is tropically forced (Peng et al. 2004). For the JJA season (panel 17c and 17d), the wave train features are still discernable, though less obvious. In the Atlantic sector and to a lesser degree the Pacific sector, there is large underestimation of the standing wave pattern causing the flow to be too zonal.

(b) SST Bias

SST climatology has been a concern in climate simulation and prediction because latent heat anomalies, a major driving force of seasonal atmospheric circulation anomalies, depend not only on the SST anomalies but also on the time-mean condition of

the ocean surface. Here we focus on the forecast bias of SST in the tropical Pacific Ocean, the most important and predictable factor affecting extratropical seasonal climate. Fig. 18 shows the 2°S-2°N average of SST bias in just the Pacific Ocean for January, April, July and October 19-23 initial conditions over the retrospective period of 23 years (1981-2003). Results from other initial days of each month are similar. There exists a large cold bias from 150°E to 110°W in target months from July to January (mainly August to October) in the forecast from January, April, and July initial conditions. A weaker cold bias is seen in target months from January to April in the forecast from July, October, and January initial conditions. Forecasts from all initial months show a warm bias close to the eastern boundary of the equatorial Pacific in target months from May to October. The causes in model physics for these SST biases are not clear. Some preliminary diagnostics indicate that the cold bias in target months from July to January in the forecast from January, April, and July initial conditions is probably associated with the too-strong easterly momentum flux in the central eastern Pacific which results in cold temperature advection.

Fig. 19 compares forecast time-mean surface momentum flux and precipitation in June from observational analysis (panel 19a) to that of the forecast from April initial conditions (panel 19b). The differences between analysis and forecast are considered to be mainly due to model physics in the atmospheric component of the CFS because tropical SST bias in the June forecast from April initial condition is small. It is seen that the easterly momentum flux errors in the forecast appear to be associated with the ITCZ precipitation band which is too strong compared to the observational CMAP analysis.

Further diagnostics and additional experiments are needed to find out which part of the model physics is responsible for the SST biases.

(c) Ocean Fields

In this section, we analyze the most important prognostic variables in the ocean, the subsurface temperature (T), zonal velocity (U), vertical velocity (W), and heat content (H), produced by the ocean component of the CFS. Our analysis focuses on the equatorial Pacific Ocean, the domain in which the regularly occurring El Nino-Southern Oscillations (ENSO) is most active. Specifically, we are interested in the faithful reproduction of the structure of the seasonal thermocline in the equatorial Pacific and the zonal velocity structure of the upper ocean. While considerable information can be gleaned from analysis of the individual members of the 15-member ensemble, we only plot and analyze ensemble mean fields in this section.

The climatological structure of the temperature field in the equatorial Pacific Ocean is plotted for the winter (DJF) and summer (JJA) seasons from GODAS in Fig. 20. The plot shows the warm pool region (> 28°C) in the Western Pacific extending to the international date-line in winter and to 160°W in summer. In winter, the 20°C isotherm, which is usually considered to be a proxy for the depth of the thermocline (McPhaden et al. 1998), shoals from approximately 160 m at its deepest point in the western Pacific (140°E) to 60 m at the eastern Pacific (Nadiga et al. 2004). In the summer, the 20°C isotherm is deeper in the western Pacific than in winter, but the situation is reversed in the eastern Pacific with the shallowest depths being less than 50m at the eastern edge of the basin. In winter, the SST are everywhere warmer than 25°C in the equatorial Pacific, but the cold tongue region extends further west than in summer. All these well-known

features are well represented in the GODAS. In the middle and bottom panels in Fig.20 (b and e), the differences between the retrospective forecasts and GODAS are plotted for winter (left) and summer (right) seasons. The color bar used in the middle and bottom panels is different from that used in the top panel, and runs from –1.5°C to 1.5°C. As shown in Fig. 20, the differences are small for the most part, and are typically less than 1°C. The greatest differences can be seen above the seasonal thermocline and in the barrier layer below the seasonal thermocline, indicating the effect of errors in vertical mixing in the ocean model. Notice that the retrospective forecasts are typically colder than GODAS, except in the region just above and below the 20°C isotherm. While the difference pattern grows from lead 3 to lead 6 for both winter and summer seasons, the difference pattern is quite different for winter and summer. We suspect the difference patterns do not result from inbuilt trends in the ocean model, but due to errors in ocean-atmosphere coupling in the retrospective forecasts. In the eastern Pacific, these forecasts are anomalously cold compared to GODAS, and this is because of too-strong vertical upwelling in that region.

Planetary waves in the equatorial Pacific Ocean play an important role in setting the periodicity and duration of ENSO events (Schopf and Suarez 1988). Thus it is important that the mean zonal velocity in the retrospective forecasts be examined for any systematic biases when compared to observations. The climatological zonal velocity in the equatorial Pacific is plotted in Fig. 21 for winter (upper left panel) and summer (upper-right panel) seasons for GODAS. The strong eastward velocities in the undercurrent are shown clearly in both seasons. The wind-driven westward velocities in the surface layer are stronger in winter than in summer, while the eastward velocities in

the undercurrent are stronger in summer. The core of the undercurrent tilts upwards and eastwards, with the largest velocities (approximately 1m s^{-1}) being reached in the core of the undercurrent at around 100 m at 140°W. Zero zonal velocities are found in regions between the North Equatorial current (NEC) and the undercurrent and below the undercurrent. In the warm pool region, strong westward currents are found in summer, possibly indicating the effect of Rossby waves impinging on the western edge of the Pacific Basin. In the middle and bottom panels, the differences between the retrospective forecasts and GODAS are plotted for leads 3 and 6 months. As was found in the temperature differences, we find that the difference patterns grow with lead time, and these patterns are quite different for summer and winter seasons. In winter, the largest differences are found in the undercurrent region, and the forecast eastward velocities are generally larger than GODAS. In the surface layers of the eastern Pacific, the wind-driven westward velocities are much larger than in GODAS, indicating that the surface fluxes are in error there.

The climatological vertical velocities in the equatorial Pacific Ocean are plotted in Fig. 22 for the winter (upper left panel) and summer (upper-right panels) for GODAS. The values shown in the figure are in mm $hour^{-1}$. The most important feature shown in the upper panels is the upwelling in the eastern Pacific. The upwelling velocities are larger in winter than in summer and reach a maximum of approximately 10 cm $hour^{-1}$. The negative vertical velocities are largest all through the water column below the warm pool, indicating the effect of downwelling Rossby waves. In both seasons, the eastward transport of mass results in strongly-positive horizontal velocity divergence in the

undercurrent region. This mass transport divergence causes strong upwelling velocities above the thermocline and strong downwelling velocities below the thermocline in the Eastern Pacific. The middle and bottom panels show differences between GODAS and retrospective forecasts for leads 3 and 6 months for winter and summer seasons. Unlike the difference plots for temperature and zonal velocity, the differences here are similar for winter and summer, indicating that errors in the divergence of surface winds and not errors in oceanic mixing are the primary cause of these differences. The most striking and noticeable feature in the middle and bottom panels is the anomalously large vertical velocities in the entire water column in the eastern Pacific. In the center of the ocean basin, anomalously large negative velocities are found. The water that upwells in the eastern part of the basin is forced westward by the surface wind stress and sinks in the center of the basin. It should be noted that because the temperatures in the surface layer in the eastern Pacific are colder in the forecasts than in GODAS (see Fig. 20), the negative heat advection due to vertical upwelling is reduced.

The heat content of the upper ocean is an important diagnostic variable in the context of seasonal weather prediction. The recharge-discharge oscillator theory (Jin 1997) holds that anomalous buildup of heat content is a prerequisite for the occurrence of El Nino, and the equatorial Pacific ocean is purged of excess heat content during the warm event. The zonally-integrated warm water volume above the 20°C isotherm has been shown to correlate closely to the Nino 3.4 SST (McPhaden 2004).

In Fig. 23, the heat content of the upper Pacific Ocean (integrated over the top 460m) is plotted for the boreal winter (upper-left panel) and summer (upper-right) seasons.

The plots show the well-known double-gyre structure in the Pacific Ocean, with the maximum values recorded in the center of the gyres. The ITCZ located at approximately 10°N demarcates the northern edge of the south Pacific gyre and the southern edge of the north Pacific gyre, with approximately 5 degrees in latitude separating the two gyres. It is clear from the plot that the warm pool region contains more thermal energy in the boreal winter than in summer. The differences between the retrospective forecasts and GODAS is plotted in the middle and bottom panels for leads 3 and 6 months and presents a heartening picture. The differences between the forecasts and GODAS are typically less than 5 % in most regions of the Pacific Ocean, and are especially small on the equator. The difference patterns are similar for winter and summer seasons and indicate that the largest errors are found in the ITCZ. The heat content in the forecasts is anomalously warm south of the ITCZ and cold north of the ITCZ, indicating that errors in the divergence of the Ekman heat flux are the cause of the heat content errors. In general, however, Fig. 23 indicates that the forecasts are able to accurately reproduce the upper ocean heat content in the equatorial Pacific ocean even for leads of 6 months and beyond. The fidelity of the forecast upper ocean heat content to the observed values is an important reason the retrospective forecast system is able to accurately predict ENSO events as is seen in Figure 24. Here, the heat content anomalies are computed and plotted for GODAS and for forecasts of leads of one, five and nine months. The anomalies were smoothed by applying a running average filter over the signal, with weights one, three and five applied to months two, one and zero before and after the current month. Fig. 24 clearly shows the three strongest warm ENSO events in the past 23 years (1982-83, 1987-89 and 1997-98). From the plots, it is clear that the heat content

anomaly was strongest for the 1982-83 and 1997-98 ENSOs in both GODAS and forecasts. The eastward propagation of the warm anomalies by downwelling Kelvin waves during the 1982-83, 1987-88, 1991-92, 1997-98 and 2000-02 warm events is accurately reproduced in GODAS and forecasts. Also, the 1983-84, 1988-89, 1998-99 cold events are reproduced accurately by the forecasts, and the lead nine month forecasts faithfully reproduce all the above events with minimal distortion. One exception is the warming in the eastern Pacific in 1995. The CFS progressively downgrades the intensity of this warming until it is no longer seen in the forecast for 9 months.

(d) Stratosphere

Although not an item of great practical interest, the forecasts for the stratosphere are a great challenge scientifically because modeling the QBO is very difficult. Fig. 25 shows the skill of stratospheric forecasts from the CFS, by looking at the status of the QBO in the model as a function of lead time from zero to eight months. While the QBO phenomenon disappears with an e-folding of close to one year in the CFS, one can still clearly see it in the eight month forecasts. This appears to be better than in previous models. Especially near 50 hPa, where there are many levels in the vertical, the forecasts of the zonal mean of the zonal wind in the tropics is considerably better than persistence (which is zero after one quarter period).

(e) Atmospheric indices

It is common to report on skill in atmospheric teleconnections patterns. Even when overall skill is low, the projection onto (observed patterns of) the North Atlantic Oscillation (NAO) and the Pacific North American pattern (PNA) may show slightly better skill by virtue of the spatial averaging implied in calculating the projections.

Indeed one can amplify the scores reported in Fig.8(top) for winter months by filtering the fields and retaining only NAO and PNA. Fig.26 shows the time series of NAO and PNA for January and February, lead 1 monthly ensemble mean forecasts, along with the observations. We find correlations of around 0.4. In other months skill is negligible. This appears consistent with results by ECMWF (Palmer et al 2005).

6. Summary, Conclusions and Discussion.

In this paper, we describe the new operational NCEP global coupled ocean-atmosphere model, called the Climate Forecast System or CFS. The component models are the 2003 NCEP atmospheric global weather prediction model, called the GFS, but at reduced resolution T62L64, and the GFDL MOM3 ocean model. The coupling is once a day using daily mean fluxes. The CFS became operational in August 2004. Apart from the countless modernizations inherent in replacing the atmospheric and ocean models by newer versions, the improvements relative to the previous coupled model include specifically (i) near global atmosphere-ocean coupling (as opposed to tropical Pacific only), (ii) a fully coupled system with no flux correction (as opposed to a 'tier-2' system with multiple bias and flux corrections), and (iii) a comprehensive set of fully coupled retrospective forecasts covering the period 1981-2004, with 15 forecasts per calendar month, for forecast leads out to nine months into the future.

Since the CFS model is used for operational seasonal prediction at CPC, the 24 year retrospective forecasts, an effort which amounts to an integration of the system for nearly 3300 years, is of paramount importance for the proper calibration of subsequent real time operational forecasts.

The CFS has an acceptably low bias in tropical SST prediction, and a level of skill in forecasting Nino3.4 SST that is comparable to statistical methods used operationally at CPC, and is a large improvement over the previous operational coupled model at NCEP. Skill in predicting SST in the mid-latitudes (not done before) is much less than in the tropics, and at longer leads there is some skill only in winter. Skill for monthly and seasonal mean temperature and precipitation over NH land, and the US in particular, is modest, but still comparable to the statistical tools used operationally at CPC and not unlike a similar model at ECMWF (Van Oldenborgh et al. 2005). Skill in precipitation is mainly in winter (ENSO related), while skill in temperature is mainly in summer, when soil moisture anomalies (initialized by Reanalysis-2, which used observed precipitation during the analysis procedure) appear helpful. Certainly the notion 'coupled' model also refers to land-atmosphere interactions.

Model behavior is reported here mainly in terms of biases or climate drift in global SST, precipitation, 200 hPa geopotential, surface wind stress, and subsurface oceanic fields. In the tropical Pacific the climate drift, while small in general, is strongest in August-September-October, even at very short lead. Some of the mid-latitude atmospheric biases appear to be forced by tropical precipitation biases. Oceanic climate drift, relative to the global ocean data assimilation, from the surface to depths of nearly 500 meters is discussed for temperature and ocean currents. In most cases, the atmospheric forcing of the ocean appears to cause climate drift in the ocean. For instance, too much upwelling in the east Pacific is caused by overly strong wind stress.

Other validation efforts of the CFS, not shown but described here, include (a) much improved tropical atmosphere-ocean, (b) reasonable variability around the model

climate, (c) apparent skill in forecasting vertical shear in the equatorial Atlantic, and (d) the prediction of the Quasi Biennial Oscillation (QBO). Wang et al (2005) have described the presence of an active tropical atmosphere in the CFS when using 64 layers (as opposed to 28 levels) in the vertical, and this choice of vertical levels was essential both for Nino3.4 SST simulation and low SST biases in the tropics. The variability of many fields has been studied. The overall standard deviation of monthly mean fields is reasonable for SST, T2m, and Z500, and the EOF for Z500 appear correct, at least for the first six (rotated) modes. For variability in precipitation and soil moisture, the results are not as good. Although the bias in winds over the equatorial Atlantic Ocean is considerable, the interannual variation in vertical wind shear in the Main Development Region (MDR) for tropical hurricanes appears promising, and the CFS operational forecasts may aid as a new tool in the making of the operational NOAA hurricane forecast for seasonal hurricane activity for the US.

The CFS retrospective forecast data lends itself to many studies that are not just related to seasonal forecasts, and we encourage the readers to use this data. The availability of data, both the retrospective forecast data and the real time operational forecast data is discussed in section 7 and links have been provided.

Seasonal forecasts at NCEP have been released to the public since about 1972. Initially these forecasts were made by old-fashioned subjective methods. During the 1980's and 90's, several formal statistical tools were added to the menu that paved the way for the use of more objective methods in seasonal prediction. In these methods, an estimate of a-priori skill, based on sufficient cross validation, could be used to weigh one tool versus another, before combining them into the official forecast. Adding numerical

forecasts that are accompanied by appreciable a-priori skill is a logical extension of this procedure. These forecasts may, or may not, have become much better, but we do have a more representative measure of a-priori skill which is vital for the proper utility of seasonal forecasts.

7. Operational Forecasts and Availability of CFS Data

The initial operational implementation of CFS involved implementation of three components : Reanalysis 2 (R2) based daily atmospheric data assimilation, a daily global ocean data assimilation, and a daily nine month long coupled model integration. The retrospective forecasts with the coupled model (discussed in the preceding sections) use R2 analysis based atmospheric initial states and R2 analysis driven assimilated global ocean states. This required NCEP to make R2 atmospheric analysis operational because it is needed for both the ocean analysis and as initial condition for the CFS forecasts. This real time operational analysis is called Climate Data Assimilation System 2 (CDAS2).

The operational global ocean data assimilation system (GODAS) uses a 28-day data window symmetrically centered around the analysis time. Thus the analysis date is 14 days behind real time. So if the GODAS analysis were to be used as the initial condition, then the daily CFS forecasts would be 14 days behind real time, which would be unacceptable. Therefore, a new asymmetric GODAS which uses only 21 days of ocean data and is valid at 7 days prior to real time was developed and implemented. This asymmetric GODAS uses the previous 28-day symmetric GODAS analysis as its first guess.

Thus, operationally three analyses are performed daily in real time: the atmospheric R2 analysis is performed with analysis time which is three days before real time, the full symmetric GODAS is performed with analysis time that is 14 days before real time and an asymmetric GODAS is performed with analysis time seven days before real time. Using this asymmetric GODAS analysis as the ocean initial state and R2 analysis valid at that time as the atmospheric state (at 00 UTC), a daily CFS forecast is made out to 9-10 months lead time. Since the operational CPC seasonal forecast is issued once a month, this strategy provides at least a 30 member ensemble of CFS forecasts to be used by the forecasters.

An additional daily CFS forecast with the same initial oceanic state and a slightly perturbed atmospheric state (by taking a weighted mean of the states corresponding to the real time date and a day earlier at 00 UTC) will soon be operational. With this addition, there will be at least a 60 member ensemble of CFS forecasts per month.

Monthly means of all variables and daily time-series of selected variables are being archived from these forecasts. The retrospective forecasts are used to correct the systematic bias from these monthly means before being used for the seasonal prediction.

The document at the following web link provides the necessary details on how to access the operational CFS forecast and retrospective climatological data from the official National Weather Service (NWS) data site:

http://www.emc.ncep.noaa.gov/gmb/ssaha/cfs_data/cfs_data.pdf

A web link provides the necessary details on how to access CFS retrospective time series data of the 53 most commonly used variables from an NCEP/EMC anonymous ftp site :

http://www.emc.ncep.noaa.gov/gmb/ssaha/cfs_data/cfs_data_in_nomad.doc

Acknowledgements

The authors would like to recognize all the scientists and technical staff of the Global Climate and Weather Modeling Branch of EMC for their hard work and dedication to the development and implementation of the GFS. We would also like to express our thanks to the scientists at GFDL for their work in developing the MOM3 ocean model. We thank Julia Zhu, Dave Michaud, Brent Gordon and Steve Gilbert from the NCEP Central Operations (NCO) for the timely implementation of the CFS in August 2004. George VandenBerghe and Carolyn Pasti from IBM are recognized for their critical support in the smooth running of the CFS retrospective forecasts and the operational implementation of the CFS on the NCEP IBM computers. We thank Curtis Marshall, EMC for his help in the editing of the manuscript and Ake Johansson and Augustin Vintzileos for many constructive comments. Finally, we thank the NOAA Office of Global Programs for the funds to obtain extra computing resources, which enabled us to complete the retrospective forecasts in a timely fashion.

References

Anderson, D. L. T., T. Stockdale, M. A. Balmaseda, L. Ferranti, F. Vitart, P. Doblas-Reyas, R. Hagedorn, T. Jung, A. Vidard, A. Troccoli, and T. Palmer, 2003: Comparison of the ECMWF seasonal forecast systems 1 and 2, including the relative performance for the 1997/8 El Ni˜no. *Technical Memoranda 404, ECMWF*, Shinfield Park, Reading, U.K. models. *Mon. Wea. Rev.*, **125**,1931-1953.

Barnston, A. G., 1994: Linear Statistical Short-Term Climate Predictive Skill in the Northern Hemisphere. *J. Climate*, **7**, 1513-1564

Barnston, A. G. and C. F. Ropelewski, 1992: Prediction of ENSO Episodes Using Canonical Correlation Analysis, *J. Climate*, **5**, 1316-1345.

Barnston, A.G., H. van den Dool, D. Rodenhuis, C.R. Ropelewski, V. E. Kousky, E. A. O'Lenic, R. E. Livezey, S. E. Zebiak, M. A. Cane, T. P. Barnett, N. E. Graham, Ji, Ming and A. Leetmaa, : 1994: Long-Lead Seasonal Forecasts—Where Do We Stand? *Bull. Amer. Meteor. Soc*., **75**, 2097-2114.

Barnston, A. G., A.Leetmaa, V. Kousky, R. Livezey, E.O'Lenic, H. Van den Dool, A.J. Wagner, D. Unger, 1999: NCEP Forecasts of the El Niño of 1997—98 and Its U.S. Impacts. *Bull. Amer. Meteor. Soc*., **80**, 1829-1852.

Barnston, A. G., S. J. Mason, L. Goddard, D. G. DeWitt and S. E. Zebiak, 2003: Multimodel ensembling in seasonal climate forecasting at IRI. *Bull. Amer. Meteor. Soc*., **84**, 1783-1796.

Behringer, D., M. Ji, and A. Leetmaa, 1998 : An improved coupled model for ENSO prediction and implications for ocean initialization. Part I: The ocean data assimilation system. *Mon. Wea. Rev*., **126**, 1013-1021.

Behringer, D. W., et al., 2005, The Global Ocean Data Assimilation System (GODAS) at NCEP, to be submitted for publication.

Derber, J.D. and A. Rosati, 1989: A global oceanic data assimilation system. *J. Phys. Oceanogr.,* **19**, 1333-1347.

Gent, P. R. and J. C. McWilliams, 1990: Isopycnal mixing in ocean circulation models. *J. Phys. Oceanogr.*, **20**, 150-155.

Griffies, S. M., A. Gnanadesikan, R. C. Pacanowski, V. Larichev, J. K. Dukowicz, and R. D. Smith, 1998: Isoneutral Diffusion in a z-Coordinate Ocean Model. *J. Phys. Oceanogr.*, **28**, 805-830.

Hong, S.-Y. and H-L. Pan, 1996: Nonlocal boundary layer vertical diffusion in a medium-range forecast model. *Mon. Wea. Rev.*, **124**, 2322-2339.

Hong, S-Y and H-L. Pan, 1998: Convective Trigger Function for a Mass-Flux Cumulus Parameterization Scheme. *Mon. Wea. Rev.*, **126**, 2599–2620.

Hou, Y-T, K. A. Campana and S-K Yang, 1996: Shortwave radiation calculations in the NCEP's global model. *International Radiation Symposium*, IRS-96, August 19-24, Fairbanks, AL.

Hou, Y., S. Moorthi,. K. Campana, 2002: Parameterization of solar radiation transfer in the NCEP models. *NCEP Office Note,* **441**. http://www.emc.ncep.noaa.gov/officenotes/FullTOC.html#2000

Ji, M., A. Kumar and A. Leetmaa, 1994: A Multiseason Climate Forecast System at the National Meteorological Center. *Bull. Amer. Meteor. Soc*., **75**, Issue 4, pp.569-578

Ji, M., A. Leetmaa and J. Derber, 1995: An ocean analysis system for seasonal to interannual climate studies. *Mon. Wea. Rev*., **123**, 460-481.

Ji, M., D. W. Behringer and A. Leetmaa, 1998 : An improved coupled model for ENSO prediction and implications for ocean initialization. Part II: The coupled model. *Mon. Wea. Rev*., **126**, 1022-1034.

Ji, M., R. Reynolds and D.W. Behringer, 2000: Use of TOPEX/Poseidon sea level data for ocean analyses and ENSO prediction: some early results, *J. Climate*, 216-231.

Jin, F.-F., An equatorial recharge paradigm for ENSO., 1997: Part I: Conceptual model. *J. Atmos. Sci.* **54**, 811-829.

Kalnay, E. and Coauthors, 1996: The NCEP/NCAR 40-year Reanalysis Project. *Bull. Amer. Meteor. Soc.*, **77**, 1057-1072.

Kanamitsu, M., W. Ebisuzaki, J. Woollen, S-K. Yang, J. J. Slingo, M. Fiorino and G. L. Potter, 2002A: NCEP–DOE AMIP-II Reanalysis (R-2) , *Bull. Amer. Meteor. Soc.*, **83**, 1631-1643.

Kanamitsu**,** M., A. Kumar**,** J-K Schemm, H-M H. Juang, W. Wang, F. Yang, S-Y Hong, P. Peng, W. Chen and M. Ji, 2002B: NCEP dynamical seasonal forecast system 2000. *Bull. Amer. Meteor. Soc.*, **83**, 1019-1037.

Kim, Y-J and A. Arakawa, 1995: Improvement of orographic gravity wave parameterization using a mesoscale gravity wave model. *J. Atmos. Sci.*, **52**, 11, 1875-1902.

Kistler, R., E. Kalnay, W. Collins, S. Saha, G. White, J. Woollen, M. Chelliah, W.Ebisuzaki, M. Kanamitsu, V. Kousky, H. van den Dool, R. Jenne, M. Fiorino,

2001: The NCEP–NCAR 50–Year Reanalysis: Monthly Means CD–ROM and Documentation. *Bull. Amer. Meteor. Soc.*, **82**, No. 2, 247–268.

Large, W. G., J. C. McWilliams, and S. C. Doney, 1994: Oceanic vertical mixing: A review and a model with nonlocal boundary layer parameterization. *Rev. Geophys.*, **32**, 363-403.

Levitus, S., R. Burgett and T. P. Boyer, 1994: *Salinity*. Vol. 3, *World Ocean Atlas 1994*, NOAA Atlas NESDIS 3, U. S. Dept. of Commerce, 99pp.

Maes, C. and D. Behringer, 2000: Using satellite-derived sea level and temperature profiles for determining the salinity variability: A new approach. *J. Geophys. Res.*, **105** (C4), 8537-8547.

Mahrt, L. and H.-L. Pan, 1984: A two-layer model of soil hydrology. *Bound.-Layer Meteorol.*, **29**, 1-20.

Manabe, S. and K. Bryan, 1969: Climate Calculations with a Combined Ocean-Atmosphere Model. *J. Atmos. Sci.*, **26**, Issue 4, 786-789.

McPhaden, M.J. and Coauthors, 1998: The Tropical Ocean Global Atmospheric (TOGA) observing system: A decade of progress. *J. Geophys. Res.*, **103** (C7), 14, 169-14, 240.

McPhaden, M.J., 2004: Evolution of the 2002/03 El Nino. *Bull. Amer. Meteor. Soc.*, 677-695.

Moorthi, S., H.-L. Pan, P. Caplan, 2001: Changes to the 2001 NCEP operational MRF/AVN global analysis/forecast system. *NWS Technical Procedures Bulletin*, **484**, pp14. [Available at http://www.nws.noaa.gov/om/tpb/484.htm].

Nadiga, S., J. Wang, D. Behringer and S. Saha, 2004: Ocean Retrospective Forecasts from the new Coupled Forecast System: 1981-2003. *Proceedings of 29th Climate Prediction and Diagnostics Workshop, Madison, WI.*

Palmer, T. N., A. Alessandri, U. Andersen, P. Cantelaube, M. Davey, P. D´el´ecluse, M. D´eque, E. Diez, F. J. Doblas-Reyes, H. Feddersen, R. Graham, S. Gualdi, J.-F. Gu´er´emy, R. Hagedorn, M. Hoshen, N. Keenlyside, M. Latif, A. Lazar, E. Maisonnave, V. Marletto, A. P. Morse, B. Orfila, P. Rogel, J.-M. Terres, and Thomson M. C., 2004/5: Development of a european multi-model ensemble system for seasonal to inter-annual prediction (DEMETER). Submitted to *Bull. Amer. Meteor. Soc*.

Pacanowski, R. C. and S. M. Griffies, 1998: *MOM 3.0 Manual*, NOAA/Geophysical Fluid Dynamics Laboratory, Princeton, USA 08542.

P. Peng, A. Kumar, Huug van den Dool, and Anthony G. Barnston, 2002: An analysis of multimodel ensemble predictions for seasonal climate anomalies. *J. Geophys. Res*., 107 (D23), 10.1029/2002JD002712.

Peng P, Q. Zhang, A. Kumar, H. van den Dool. W. Wang, S. Saha and H-L. Pan, 2004: Variability, predictability and prediction of DJF season climate in CFS. *Proceedings of 29th Climate Prediction and Diagnostics Workshop, Madison, WI.*

Reynolds, R. W. and T. M. Smith, 1994: Improved global sea surface analyses using optimum interpolation. *J. Climate*, **7**, 929-948.

Reynolds, R.W., N. A. Rayner, T. M. Smith, D. C. Stokes and W. Wang, 2002: An improved in situ and satellite SST analysis for climate. *J. Climate*, **15**, 1609-1625.

Saha, S. ,2004: Validation of the NCEP CFS forecasts. *Proceedings of 29th Climate Prediction and Diagnostics Workshop, Madison, WI.*

Schopf, P.S. and M.J. Suarez, 1988: Vacillations in a coupled ocean-atmosphere model. *J. Atmos. Sci*., **45**, 549-566.

Smagorinsky, J. 1963: General circulation experiments with the primitive equations: I. The basic experiment. *Mon. Wea. Rev.*, **91**, 99-164.

Stockdale, T. N., D. L. T. Anderson, J. O. S. Alves, and M. A. Balmaseda, 1998: Global seasonal rainfall forecasts using a coupled ocean–atmosphere model. *Nature*, **392,** 370–373.

Sundqvist, H., E. Berge, and J. E. Kristjansson, 1989: Condensation and cloud studies with mesoscale numerical weather prediction model. *Mon. Wea. Rev.,* **117**, 1641-1757.

Unger, D., A. Barnston, H. Van den Dool, and V. Kousky, 1996: Consolidated forecasts of tropical Pacific SST in Niño 3.4 using two dynamical models and two statistical models. *Experimental Long-Lead Forecast Bulletin*. **5,** No. 1, 50–52.

Van den Dool, H. M.,1994: Searching for analogues, how long must one wait? *Tellus*, **46A**, 314-324.

Van den Dool, H. M. and A. G. Barnston, 1994: Forecasts of Global Sea Surface Temperature out to a Year using the Constructed Analogue Method. *Proceedings of 19 th Climate Diagnostics Workshop,* College Park, MD, November 14-18, 1994, 416-419.

Van den Dool, H. M. and L. Rukhovets, 1994: On the weights for an ensemble averaged 6-10 day forecast at NMC. *Weather and Forecasting*. ,**9**, 457-465.

Van Oldenborgh, G. J., M. A. Balmaseda, L. Ferranti, T. N. Stockdale and D. L. T. Anderson, 2005: Did the ECMWF seasonal forecast model outperform a statistical model over the last 15 years? *ECMWF Technical Memorandum*, **418.**

Wang, W., S. Saha, H.-L. Pan, S. Nadiga, and G. White, 2005: Simulation of ENSO in the new NCEP Coupled Forecast System Model. Accepted by *Mon. Wea. Rev*.

Xie, P., and P.A. Arkin, 1997: Global precipitation: A 17-year monthly analysis based on gauge observations, satellite estimates, and numerical model outputs. *Bull. Amer. Meteor. Soc.,* **78**, 2539 - 2558.

Xue, Y., A. Leetmaa, and M. Ji, 2000: ENSO Prediction with Markov Models: The Impact of Sea Level , *J. Climate*, **13**, 849-871.

Zhao, Q. Y., and F. H. Carr, 1997: A prognostic cloud scheme for operational NWP models. *Mon. Wea. Rev.*, **125**,1931-1953.

Appendix : Anomaly Correlation, Systematic Error Correction and Cross Validation.

The anomaly correlation is defined as:

$$AC = \frac{\sum\sum X'_{for}(s,t)\ X'_{obs}(s,t) / nst}{[\sum\sum X'_{for}(s,t)\ X'_{for}(s,t) / nst\ .\ \sum\sum X'_{obs}(s,t)\ X'_{obs}(s,t) / nst\ ]^{1/2}} \quad (1)$$

where, for a given lead and forecast target month/season, the summation is both over time (generally 23 cases (years)), space (e.g. the grid points north of 35^oN ; cosine weighting (not shown) is used in that case), and potentially even a third summation over ensemble members. nst is the number of space-time points. The primed quantities X' (X can be any variable, or ensemble mean of a variable) are defined as $X' = X - C_{obs}$ where C_{obs} is the observed climatology. In the traditional definition of AC, the same observed climatology C_{obs} is removed from both forecast X_{for} and observation X_{obs}. Thus, the climatology could refer to any set of (previous 30) years (like 1971-2000) over which the climatology is traditionally calculated. In many modern studies it may seem natural, at first, to remove the model climatology C_{mdl}, if available, from X_{for} , i.e $X'_{for} = X_{for} - C_{mdl.}$ This approach can also be written $X'_{for} = X_{for} - C^*_{obs} - (C_{mdl} - C^*_{obs})$ by adding and subtracting the term C^*_{obs}, which is an observed climatology computed over the same set of years as the model climatology . The expression in parentheses is the systematic error correction, as evaluated over common years (here 1981-2003 or 1982-2004 for longer lead forecasts starting beyond May). One might say that subtracting the model climatology from X_{for} ,instead of the observed climatology, is an implicit correction for the systematic error. If we use common years (e.g.1981-2003) for the observed and model climatology in equation (1) i.e. $C^*_{obs} = C_{obs}$, then the interpretation of equation

(1) is simplified and using $X'_{for} = X_{for} - C_{mdl}$ and $X'_{obs} = X_{obs} - C^*_{obs}$ in equation (1) amounts to a verification of systematic error corrected forecasts. In general, however, $C^*_{obs} \neq C_{obs}$ and thus the systematic error corrected X'_{for} in equation (1) should be kept as $X'_{for} = X_{for} - C_{obs} - (C_{mdl} - C^*_{obs})$. Furthermore, because of the implied systematic error correction, one needs to do a proper cross-validation, i.e. not use information about the year to be verified in the determination of the systematic error correction (which would amount to 'cheating'). This creates some complication in programming equation (1). The summation in time requires an 'outer loop', where each year is withheld in turn. Thus, the computation of $X'_{for}(t) = X_{for}(t) - C_{obs} - (C_{mdl} - C^*_{obs})$ and $X'_{obs}(t) = X_{obs}(t) - C_{obs}$ for specific time 't' requires an adjusted C_{mdl} and C^*_{obs} (and possibly C_{obs}) such that the year 't' is not part of the various climatologies that are being computed. This cross validation is important for all verification of retrospective forecasts using anomaly correlation, rms-error and other skill measures.

Figure Legends

Fig.1 Anomaly correlation (%) of CFS ensemble mean forecasts of the monthly mean Nino3.4 SST over the period 1981-2003, as a function of target month and lead (in months). Nino3.4 is defined as the spatial mean SST over 5^oS-5^oN and 170^oW-120^oW. Example, the anomaly correlation for a lead 3 forecast for March (made from 15 initial conditions beginning Nov 9th and ending Dec 3rd) is 0.81. Keep in mind that the spatial averaging increases the correlation relative to the traditional verification at grid points in the domain.

Fig.2 Anomaly correlation (%) by various methods of the seasonal mean Nino3.4 SST as a function of lead (in months). The results are accumulated for all seasons in the (target) period DJF 1997/98 to DJF 2003/04. Except for CFS, all forecasts were archived in real time at CPC. CMP14 is the previous coupled model, CCA is canonical correlation analysis, CA is constructed analogue, CON is a consolidation (a weighted mean), and MARKOV is an autoregressive method (see text for references).

Fig.3 As Fig. 1 but now a 'verification' of the ensemble mean CFS (N-1 members) verified against the remaining single member. This is a predictability estimate under perfect model assumptions . Note the much reduced spring barrier.

Fig.4 Time series 1981-2003 of Nino3.4 SST (degree C) in November. Observations in the top panel and 6 month lead forecasts by CFS, CA and CMP14. The anomaly

correlation over the period is shown in the legend of each figure. Note that CFS has better amplitude than CA and CMP14. The forecasts should be considered retrospective in the years before the respective methods became operational, i.e. before 2003 for CFS, and before about 1997 for CA and CMP14.

Fig.5 As Fig.1 but now SST grid points in Northern Hemisphere mid-latitudes (>=35^{o}N). No spatial averaging of SST is done here.

Fig.6 As Fig.3 but now potential predictability for SST in the NH (>=35^{o}N).

Fig.7 Anomaly correlation (in %) of ensemble mean CFS forecasts as a function of lead and target month for monthly mean temperature (top) and precipitation (bottom) over land in the NH (>=22.5^{o}N).

Fig. 8 The same as Fig.7, but now 500 hPa geopotential (top) and soil moisture (upper 2m). Soil moisture is over land (>=22.5^{o}N) while 500 hPa geopotential is taken north of 35^{o}N.

Fig 9 Spatial distribution of retrospective forecast skill (anomaly correlation in %) over the United States for lead 1 seasonal mean JJA temperature (left panel) and DJF temperature (right panel). From top to bottom, the number of members in the CFS ensemble mean increases from 5 to 15. Values less than 0.3 (deemed insignificant) are not shown. The period is 1981-2003

Fig. 10 As Fig.9, but now for precipitation.

Fig.11 Left column: Spatial distribution of retrospective ensemble mean CFS forecast skill (anomaly correlation in %) for lead 1 seasonal mean temperature over the United States. The target seasons are, from top to bottom, MAM, JJA, SON and DJF. The CFS (left) is compared to CCA, in the right column. Note that CCA is based on a longer period, 1948-2003. Correlation less than 0.3 are not shown.

Fig. 12 The same as Fig.11, but now precipitation.

Fig. 13 Anomaly correlation (in %) of ensemble mean CFS forecasts as a function of lead and target month for monthly mean temperature over four quadrants of the United States (using 100^{o}W and 40^{o}N to define quadrants), evaluated only over those instances during 1981-2003 when an anomaly larger than 2 standard deviation occurred in the observations (anywhere in the quadrant). The much reduced sample size (relative to Fig.7 and 8), causes noisy patterns.

Fig. 14 The same as Fig. 13, but now precipitation.

Fig.15. Observed climatology and the CFS model climate drift for SST. The climatology is defined over the period of 1982-2004. The climate drift is obtained by subtracting the observed climatology from the model forecast climatology. Left

panels are for the winter season (DJF) and right panels are for the summer season (JJA). The top panels are the observed climatology. The middle and lower panels are the model climate drift for the 3-month lead and the 6-month lead, respectively. Unit is ^{o}C

Fig.16. Same as Fig.15 but for precipitation rate. Unit is mm/day

Fig. 17. Same as Fig.15 but for 200hPa geopotential height. Unit is meter.

Fig. 18. Climate drift (Bias) of 2^{o}S-2^{o}N average SSTs in the Pacific for forecast from initial conditions of (a) January, (b) April, (c) July, and (d) October. Contours are drawn at 0.5 K interval. Negative values are shaded.

Fig. 19. Precipitation rate (color shadings) and surface momentum flux (vectors) of June from (a) R2/CMAP, and (b) forecast from April initial condition. Contours are the amplitude of surface momentum flux (0.1 N m^{-2}). Precipitation rate is shaded at 1, 2, 4, 8, 16, and 20 mm day^{-1}.

Fig. 20: The climatology of GODAS subsurface temperature in a depth-longitude cross section along the Equator in the Pacific and mean difference between the forecasts and GODAS in degrees Celsius. The figures on the left are for boreal winter (DJF), while the figures on the right are for boreal summer (JJA). The top panels

show the climatology of subsurface temperature from GODAS. Note that a different scale is used for the color bar in the top panel.

Fig. 21: As Fig. 20 but now zonal velocity in cm/s.

Fig. 22: As Fig. 20, but now vertical velocity in mm/hour.

Fig. 23: As Fig. 20, but now a latitude/longitude representation of the upper ocean heat content in 10^7 J m^{-2}.

Fig. 24 Longitude-time plots of heat content anomalies along the equator in the Pacific from GODAS and CFS retrospective predictions. The climatology was computed for the period: 1982-2003. Unit is 10^7 J m^{-2}.

Fig. 25: Anomaly correlation of Zonal mean zonal wind anomaly at the equator as a function of pressure level (above 100 hPa) versus forecast lead time (in months).

Fig. 26 An evaluation of skill in the NAO and PNA index for January and February at lead 1. The forecast values (ensemble mean) are multiplied by 2.5 for the purpose showing realistic magnitude in the anomalies.

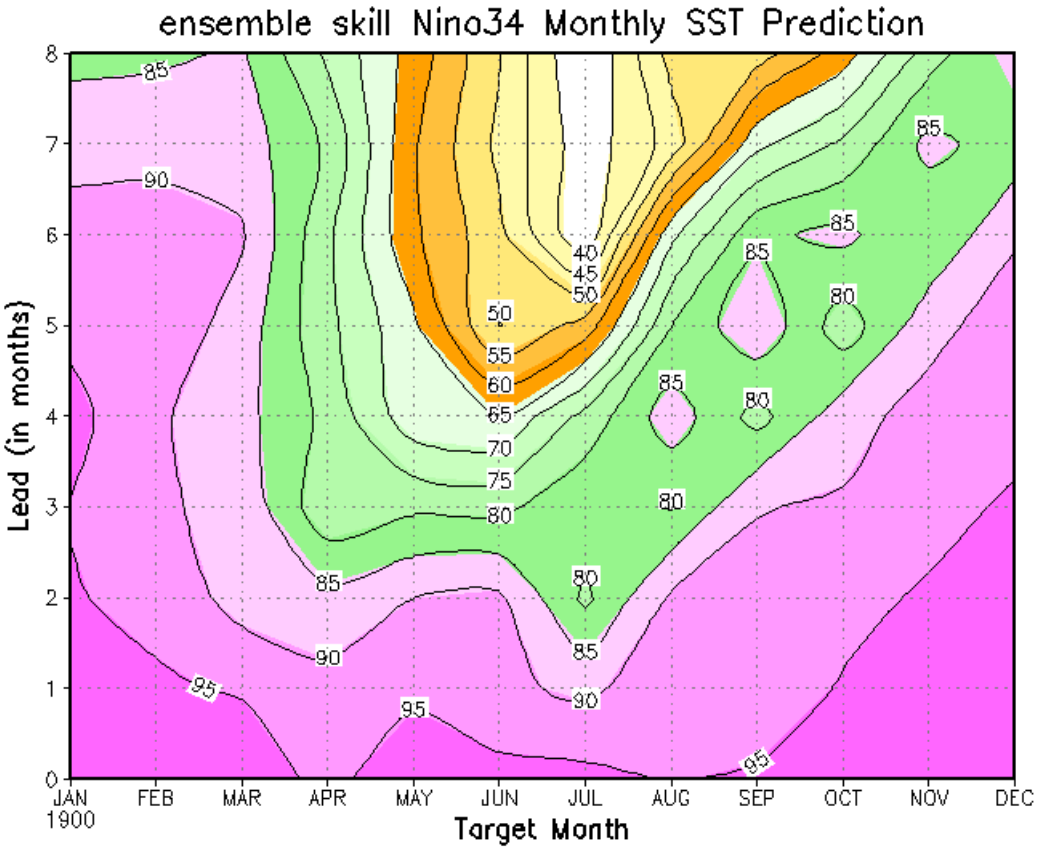

Fig. 1 Anomaly correlation (%) of CFS ensemble mean forecasts of the monthly mean NINO3.4 SST over the period 1981-2003, as a function of target month and lead (in months). Nino3.4 is defined as the spatial mean SST over 5^{o}S-5^{o}N and 170^{o}W-120^{o}W. Example, the anomaly correlation for a lead 3 forecast for March (made from 15 initial conditions beginning Nov 9th and ending Dec 3rd) is 0.81. Keep in mind that the spatial averaging increases the correlation relative to the traditional verification at grid points in the domain.

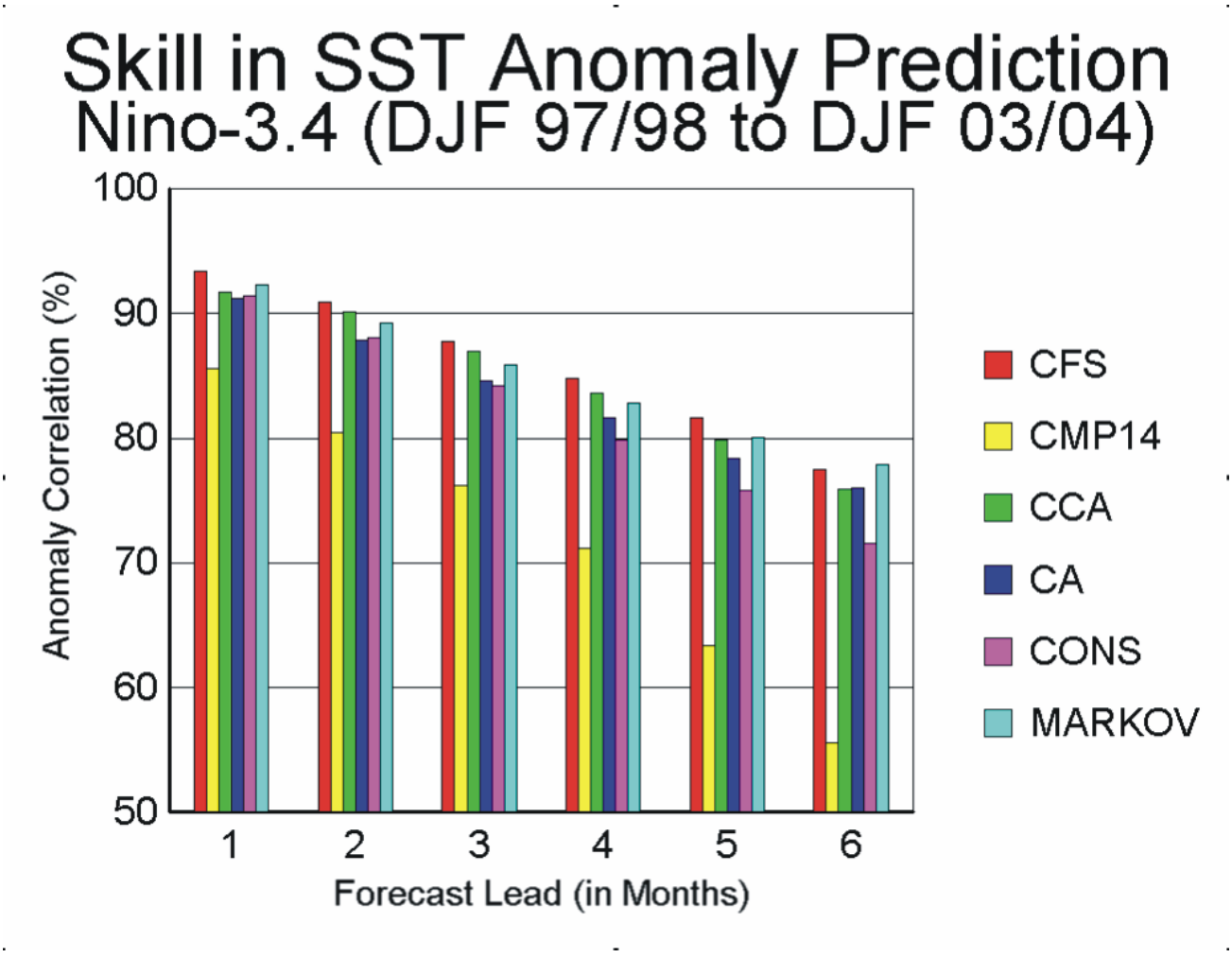

Fig. 2 Anomaly correlation (%) by various methods of the seasonal mean Nino3.4 SST as a function of lead (in months). The results are accumulated for all seasons in the (target) period DJF 1997/98 to DJF 2003/04. Except for CFS, all forecasts were archived in real time at CPC. CMP14 is the previous coupled model, CCA is canonical correlation analysis, CA is constructed analogue, CON is a consolidation (a weighted mean), and MARKOV is an autoregressive method (see text for references).

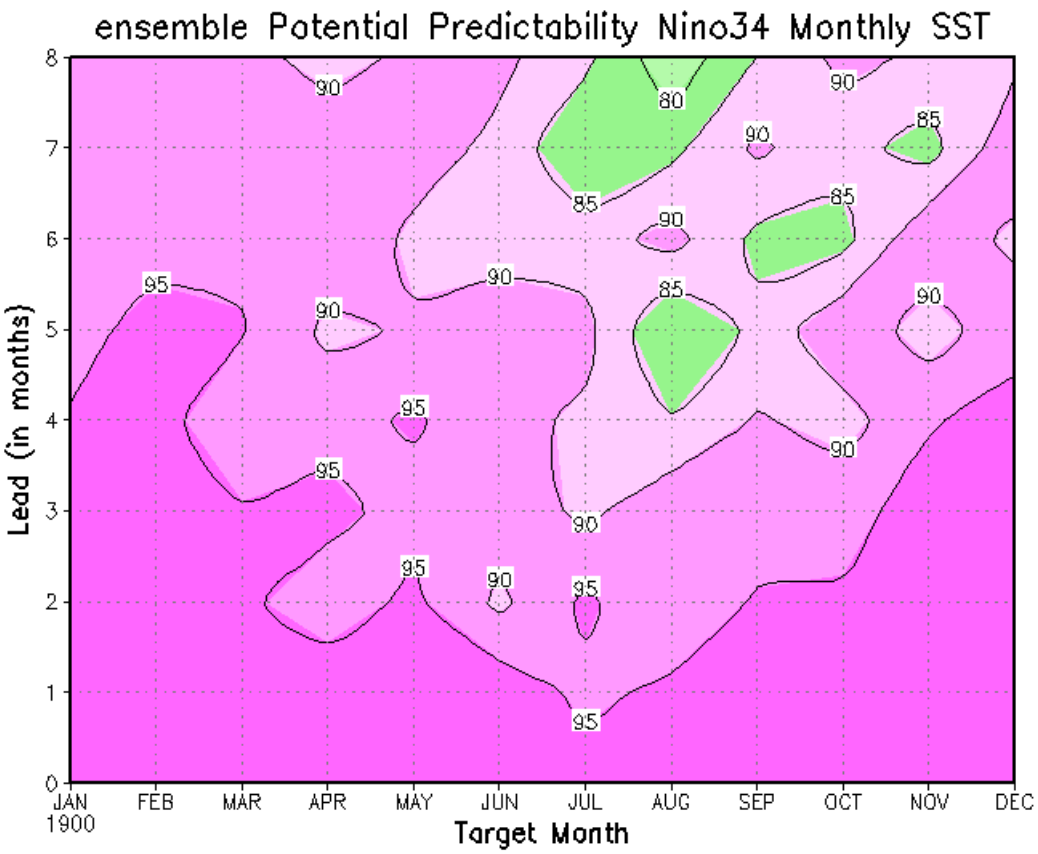

Fig. 3 As in Fig. 1 but now a "verification" of the ensemble mean CFS (N-1 members) verified against the remaining single member. This is a predictability estimate under perfect model assumptions . Note the much reduced spring barrier.

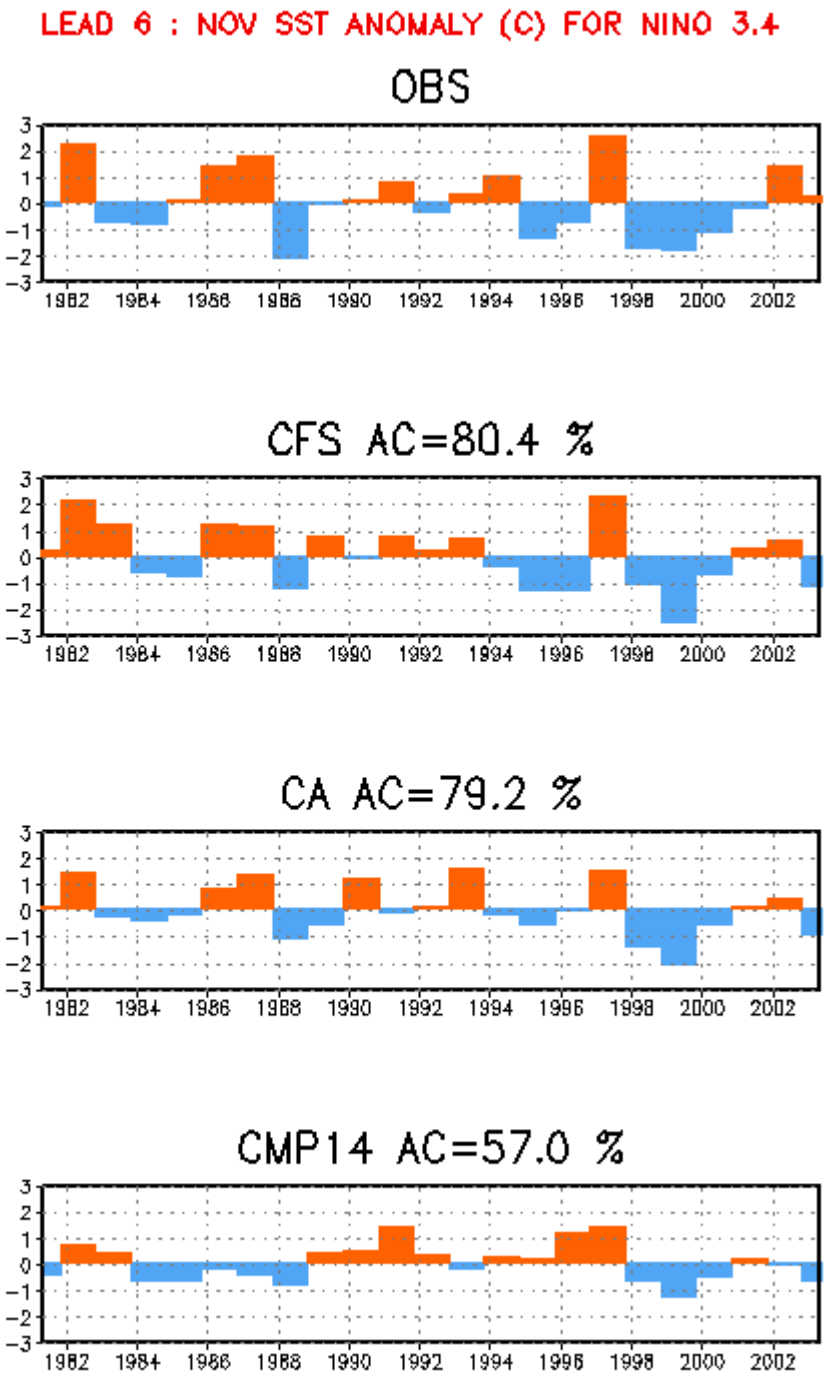

Fig. 4 Time series of Nino3.4 SST (^{o}C) in November. Observations in the top panel and 6 month lead forecasts by CFS, CA and CMP14. The anomaly correlation over the period is shown in the legend of each figure. Note that CFS has better amplitude than CA and CMP14. The forecasts should be considered retrospective in the years before the respective methods became operational, i.e. before 2003 for CFS, and before about 1997 for CA and CMP14.

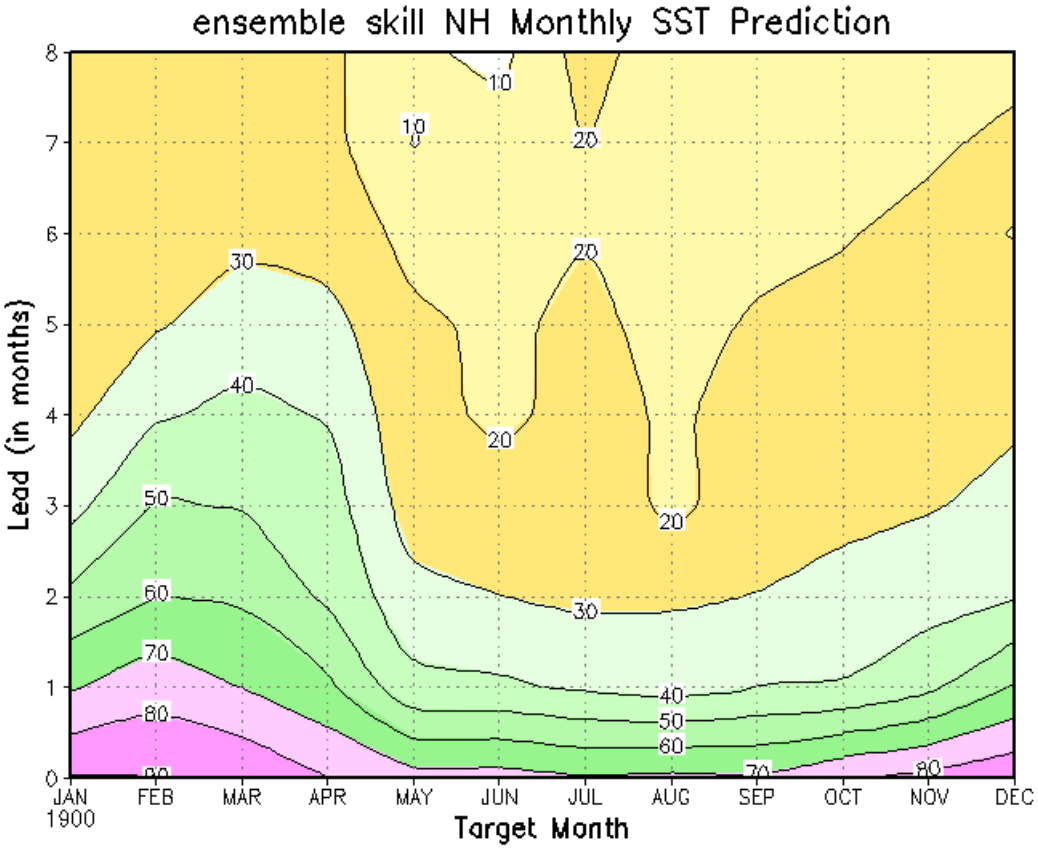

Fig. 5 As in Fig.1 but now SST grid points in NH mid-latitudes (>=35^{o}N). No spatial averaging of SST is done here.

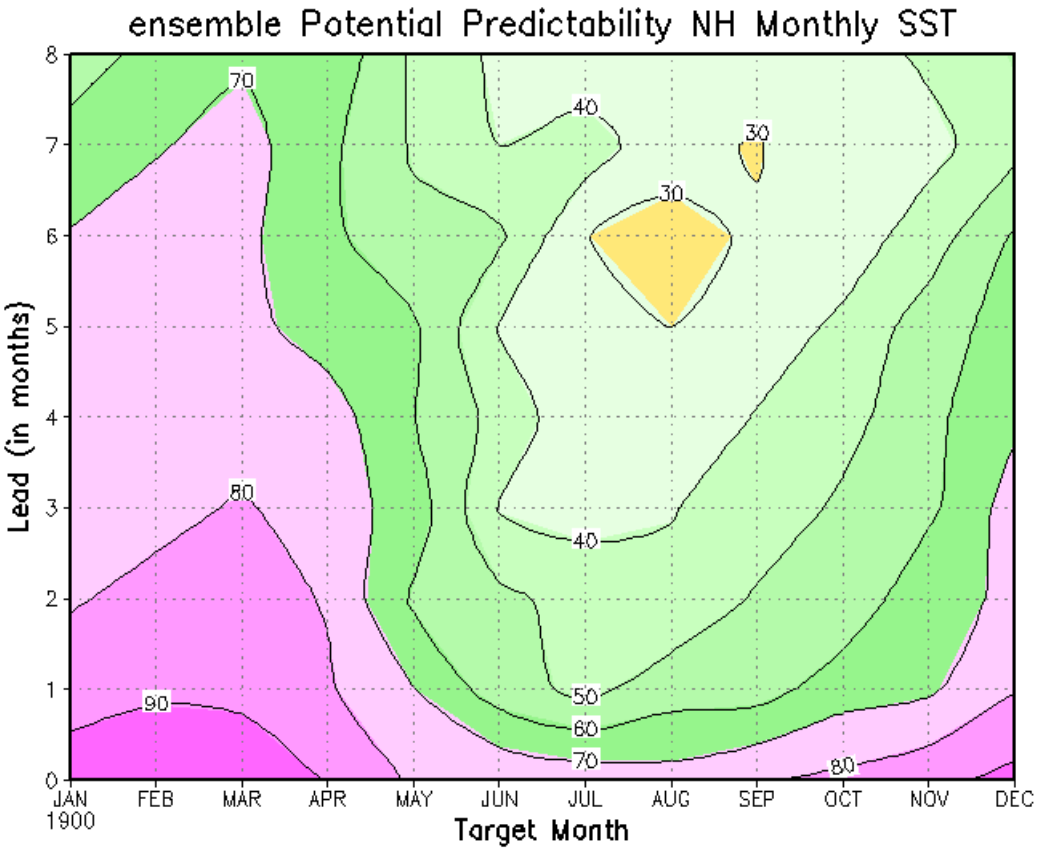

Fig. 6 As in Fig.3 but now potential predictability for SST in the NH (>=35^{o}N).

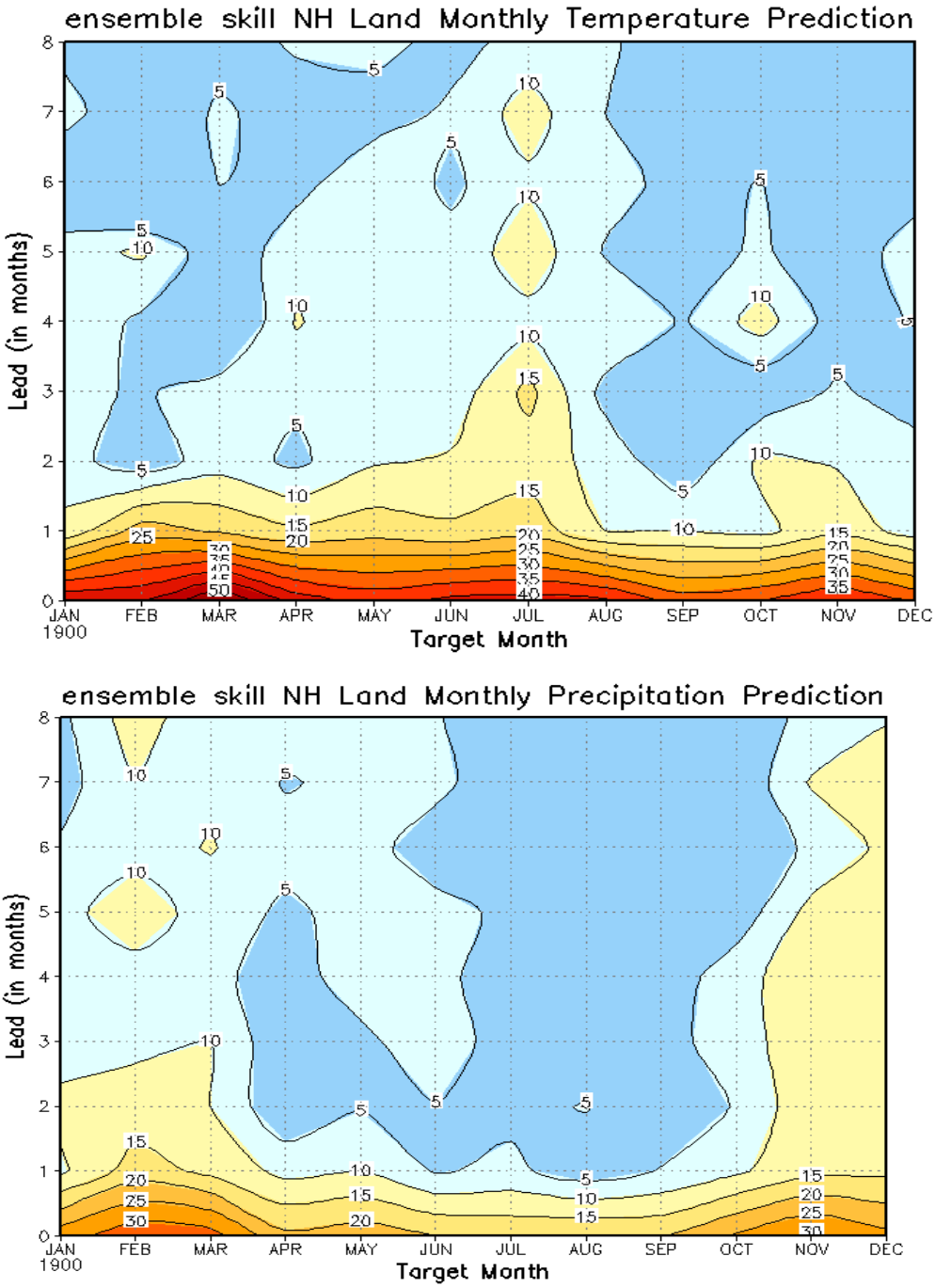

Fig. 7: Anomaly correlation (in %) of ensemble mean CFS forecasts as a function of lead and target month for monthly mean temperature (top) and precipitation (bottom) over land in the NH (>=22.5^{o}N).

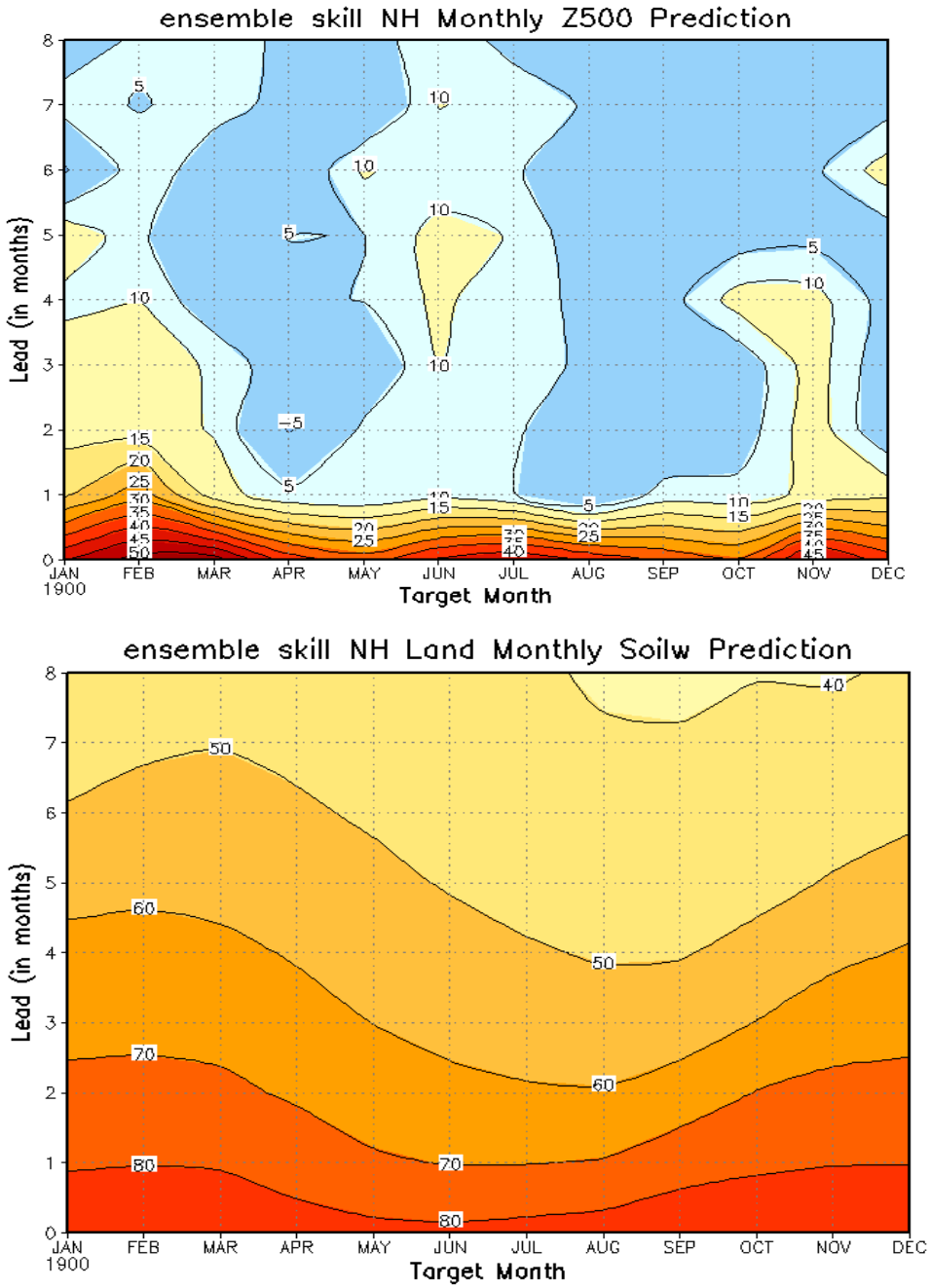

Fig. 8 As in Fig.7, but now 500mb height (top) and soil moisture (upper 2m). Soil moisture is over land (>=22.5^{o}N) while 500mb height is taken north of 35^{o}N.

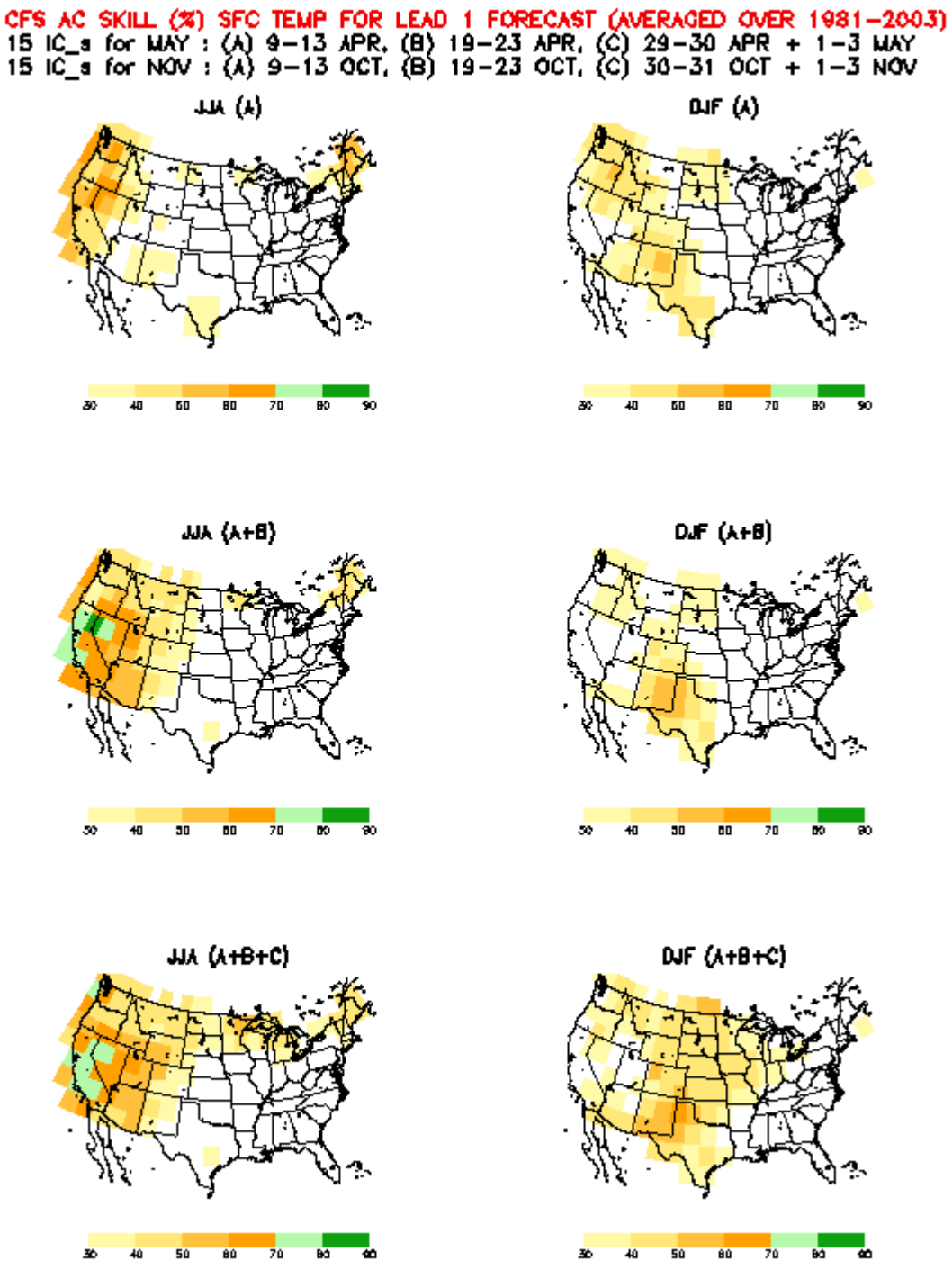

Fig. 9 Spatial distribution of retrospective forecast skill (anomaly correlation in %) over the United States for lead 1 seasonal mean JJA temperature (left panel) and DJF temperature (right panel). From top to bottom, the number of members in the CFS ensemble mean increases from 5 to 15. Values less than 0.3 (deemed insignificant) are not shown. The period is 1981-2003.

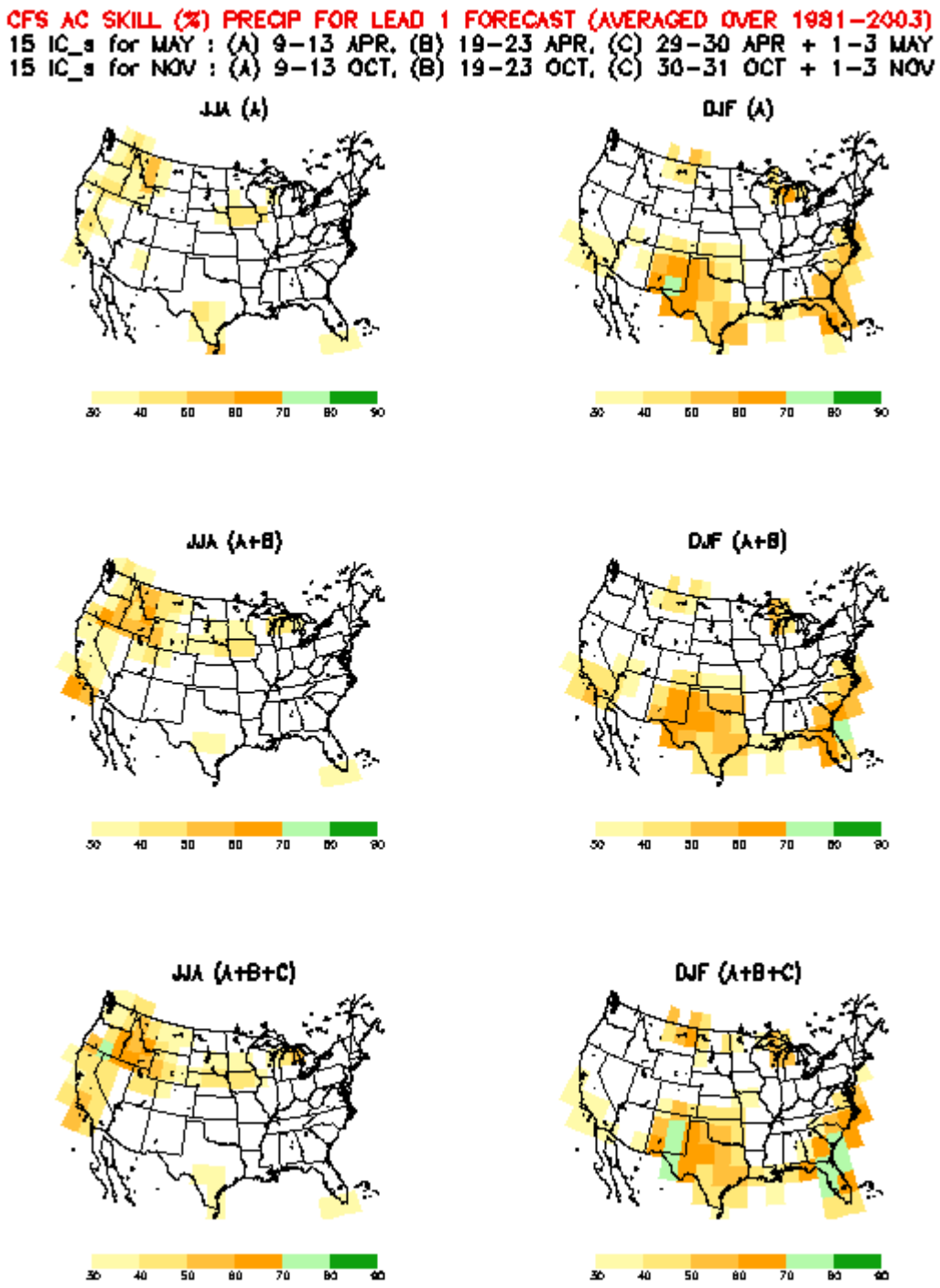

Fig. 10 As in Fig.9, but now for Precipitation.

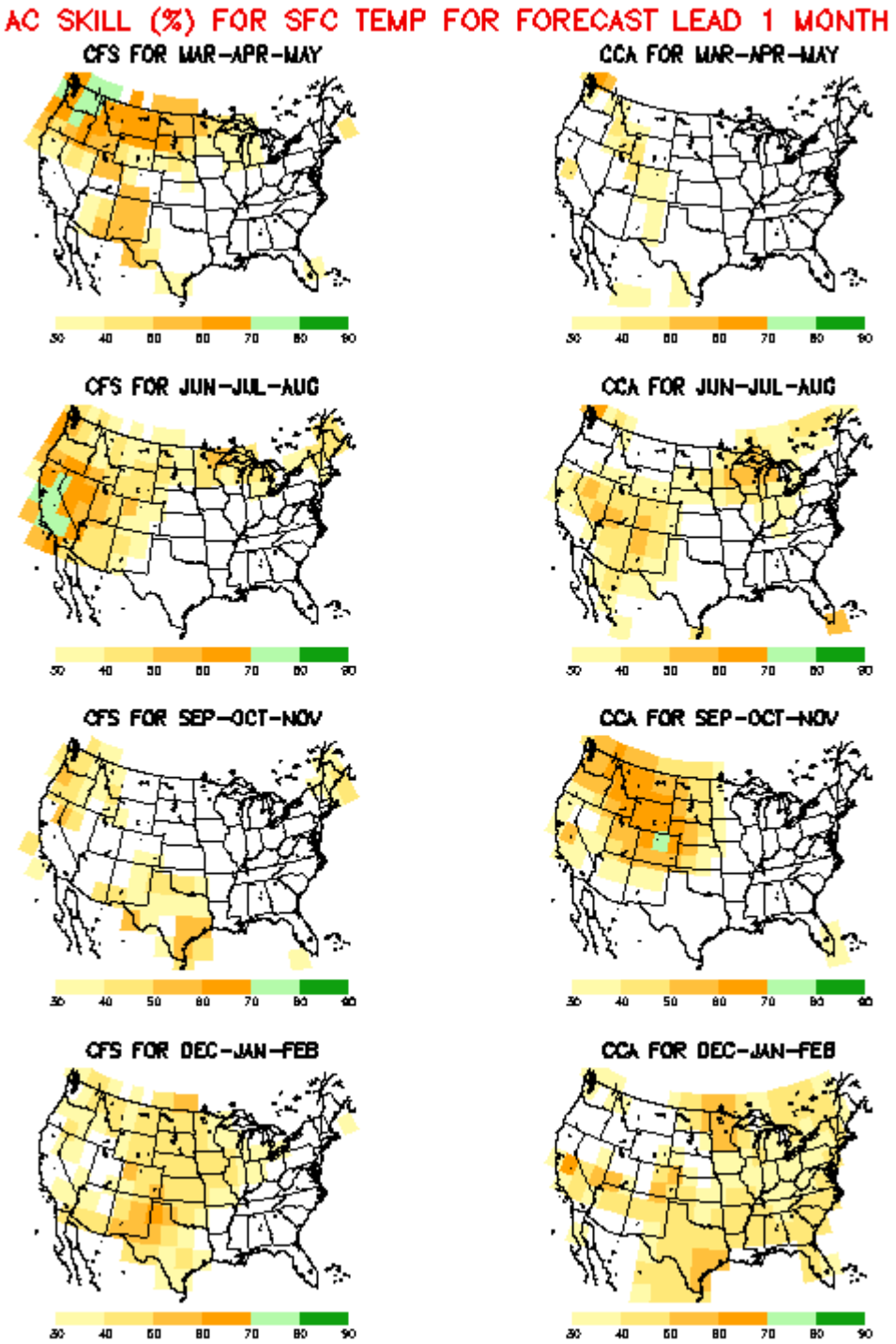

Fig. 11 Left column: Spatial distribution of retrospective ensemble mean CFS forecast skill (anomaly correlation in %) for lead 1 seasonal mean temperature over the United States. The target seasons are, from top to bottom, MAM, JJA, SON and DJF. The CFS (left) is compared to CCA, in the right column. Note that CCA is based on a longer period, 1948-2003. Correlation less than 0.3 are not shown.

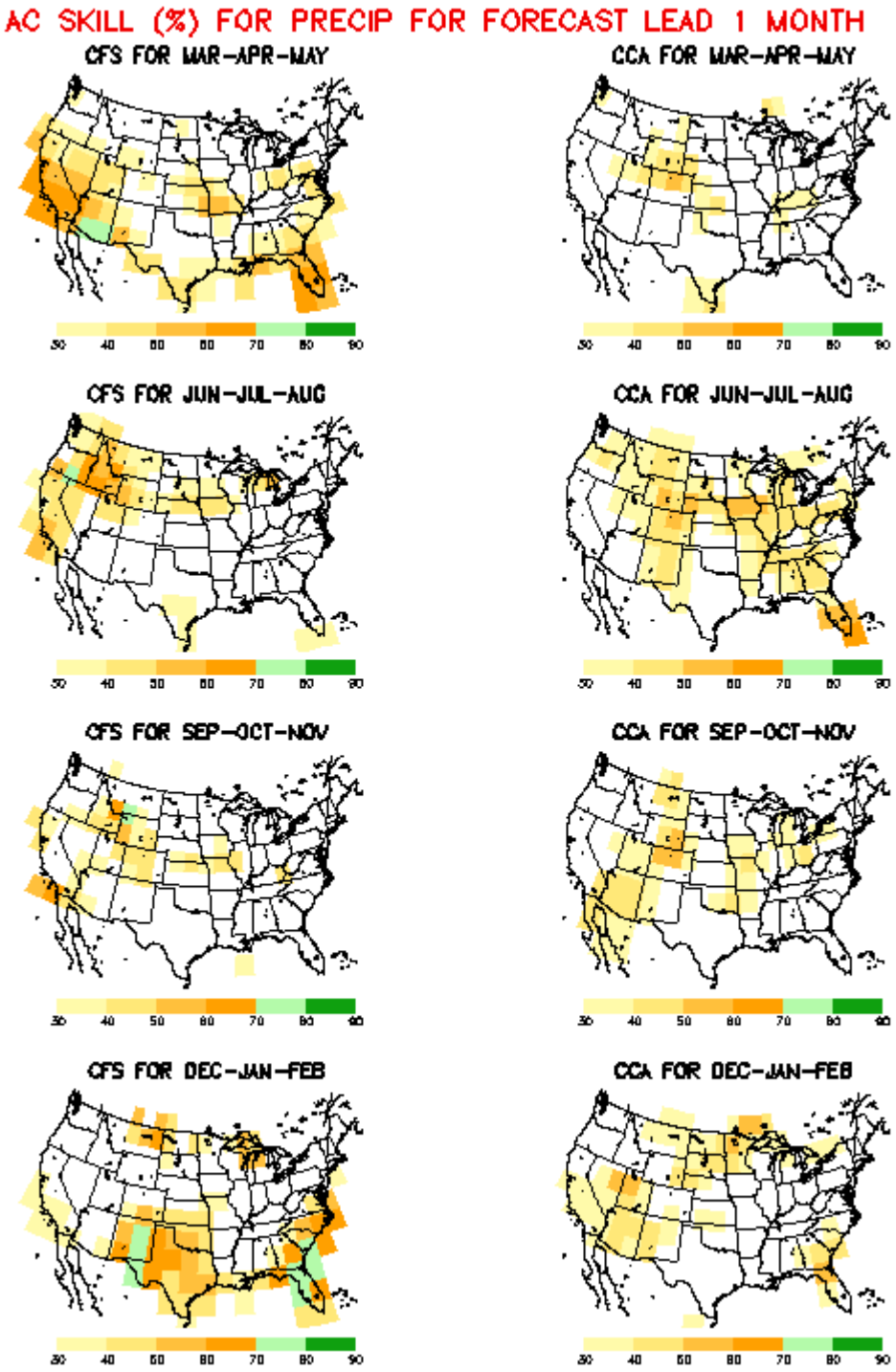

Fig. 12 As in Fig.11, but now for precipitation.

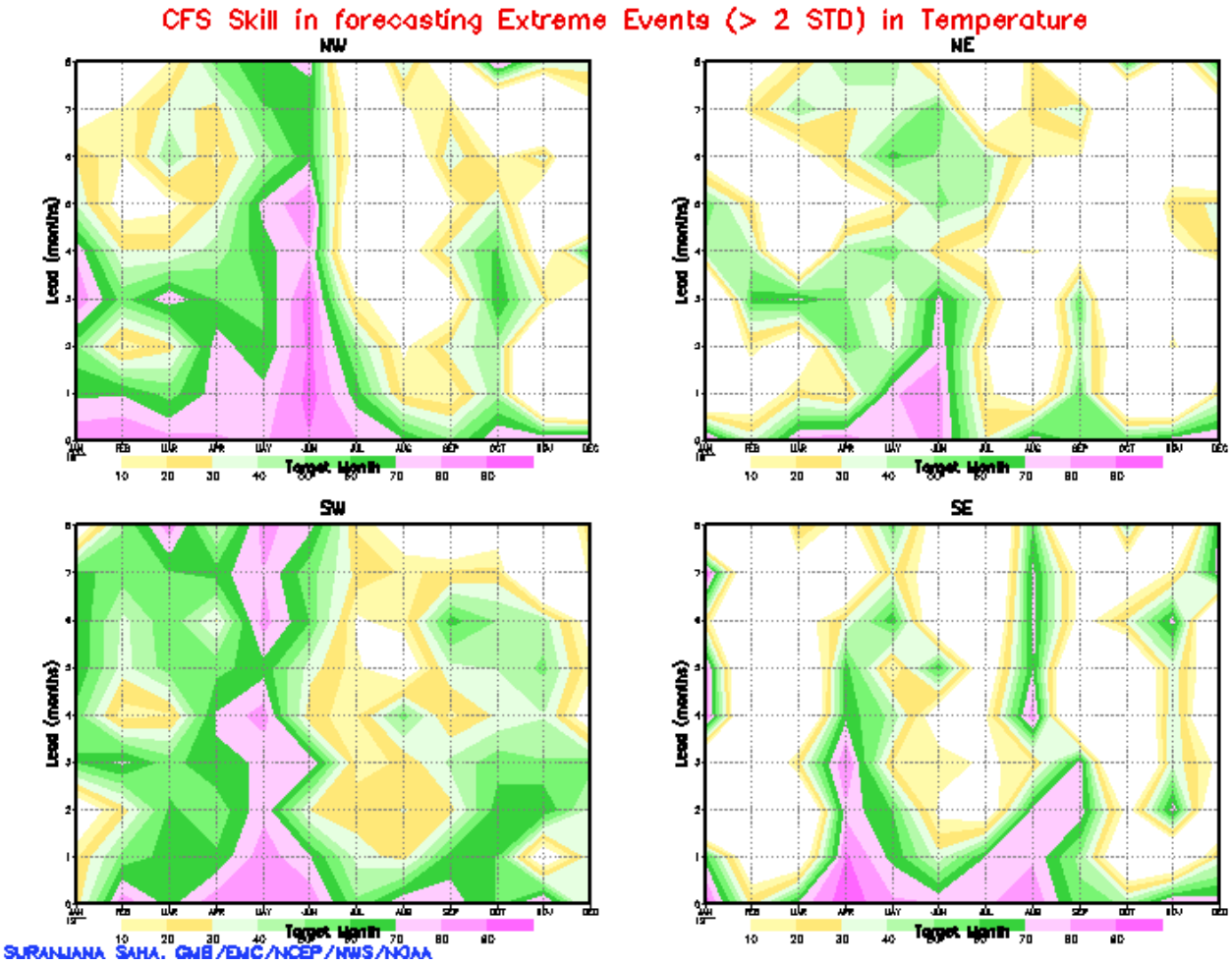

Fig.13 Anomaly correlation (%) of ensemble mean CFS forecasts as a function of lead and target month for monthly mean temperature over four quadrants of the United States (using 100^{o}W and 40^{o}N to define quadrants), evaluated only over those instances during 1981-2003 when an anomaly larger than 2 standard deviation occurred in the observations (anywhere in the quadrant). The much reduced sample size (relative to Fig.7 and 8), causes noisier patterns.

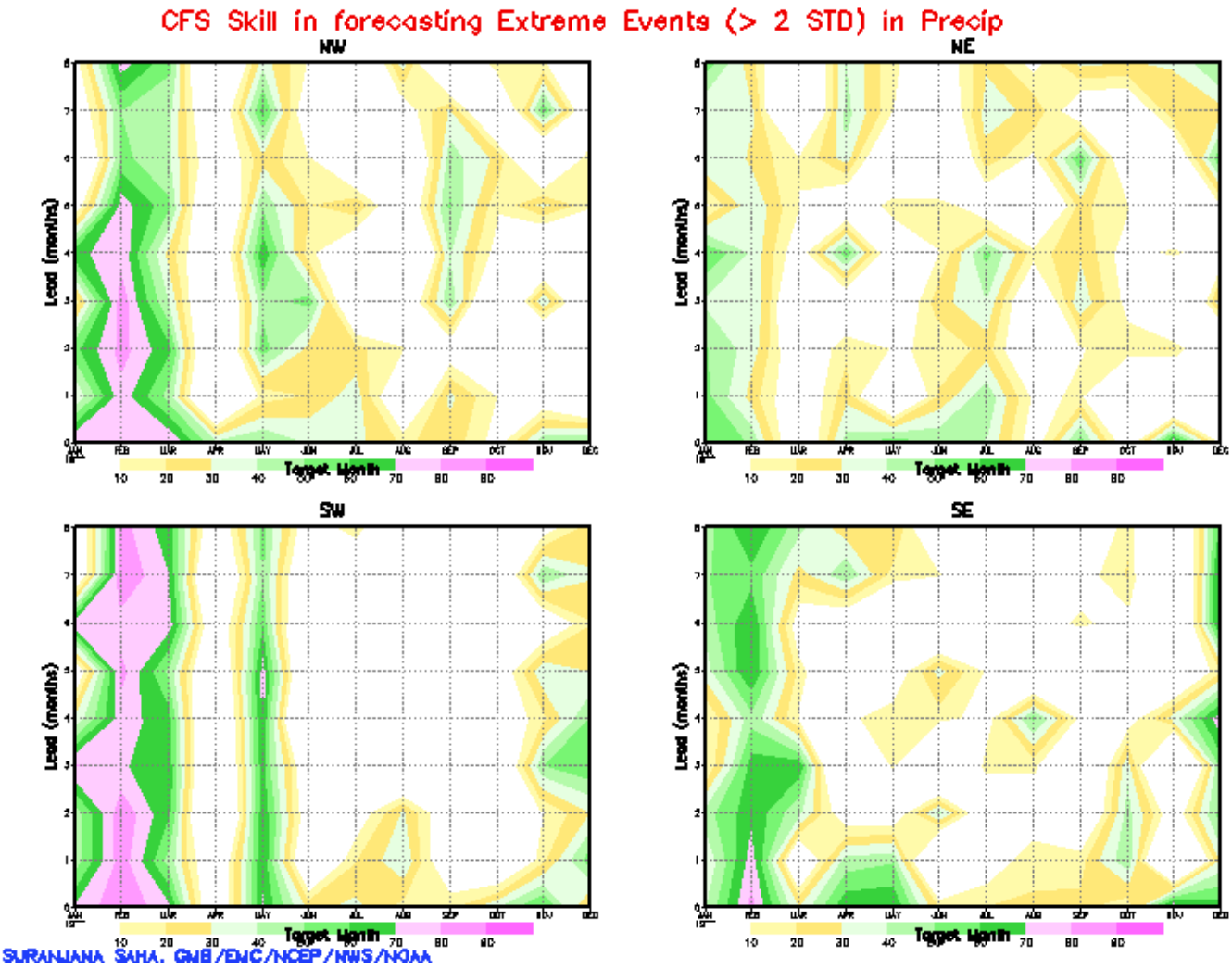

Fig. 14 As in Fig. 13, but now for precipitation.

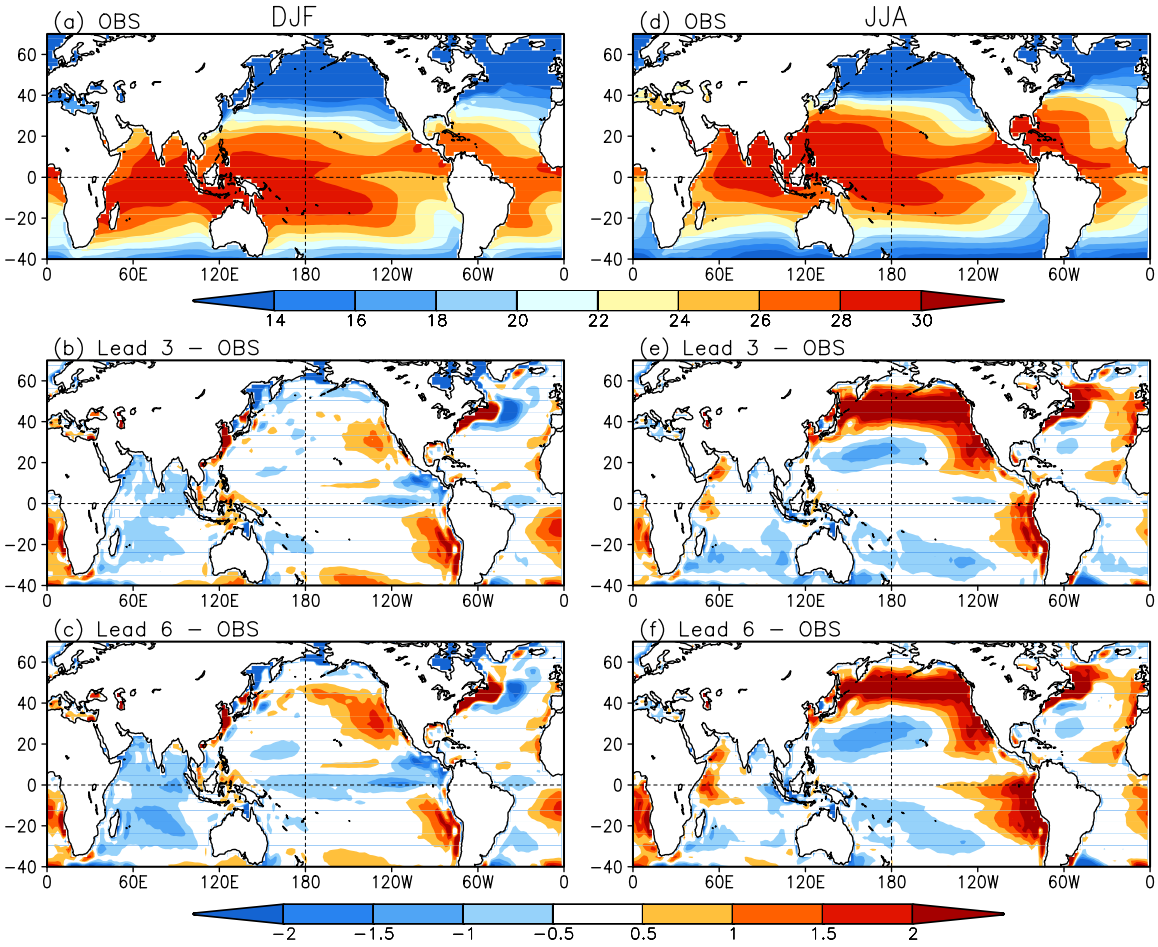

Fig.15. Observed climatology and the CFS model climate drift for SST. The climatology is defined over the period of 1982-2004. The climate drift is obtained by subtracting the observed climatology from the model forecast climatology. Left panels are for the winter season (DJF) and right panels are for the summer season (JJA). The top panels are the observed climatology. The middle and lower panels are the model climate drift for the 3-month lead and the 6-month lead, respectively. Unit is ^{o}C.

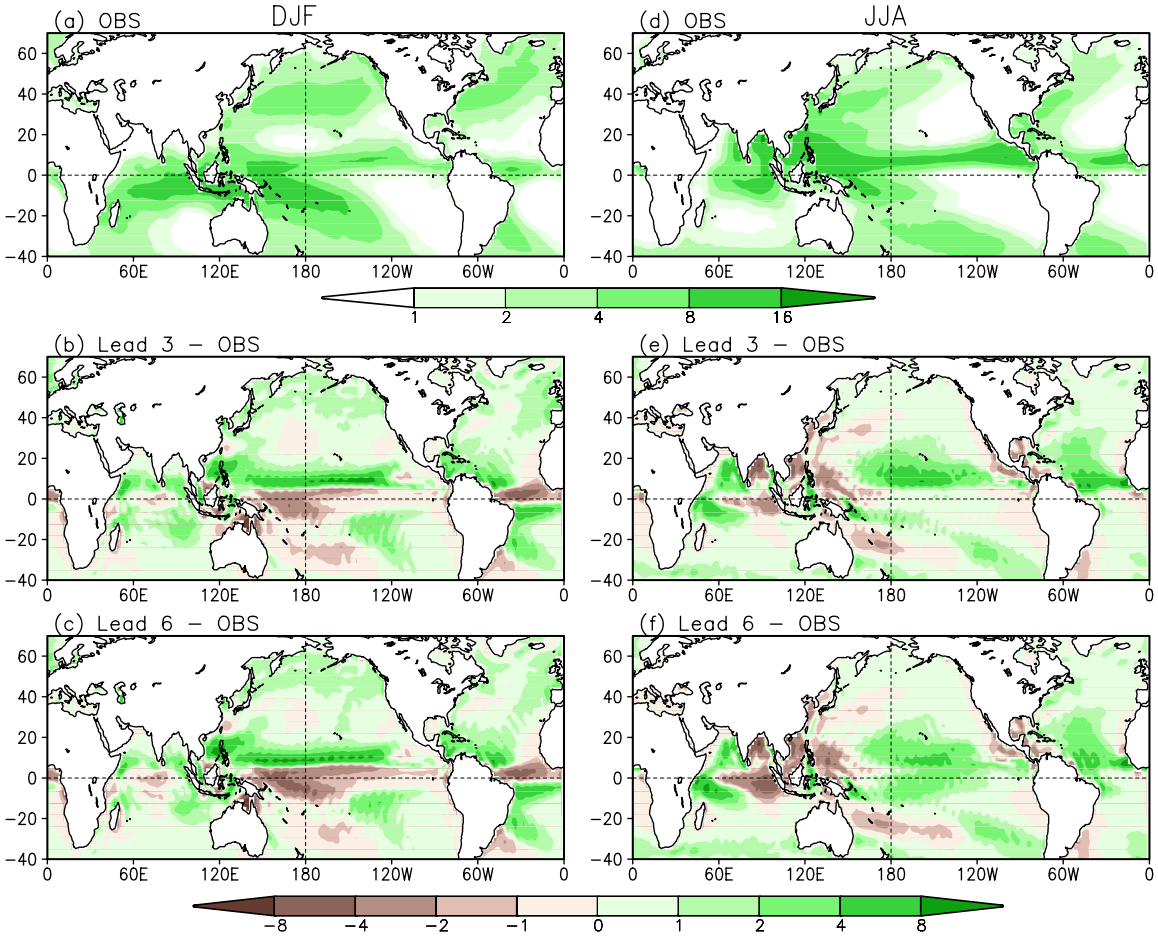

Fig.16. As in Fig.15 but for precipitation rate. Unit is mm day^{-1}.

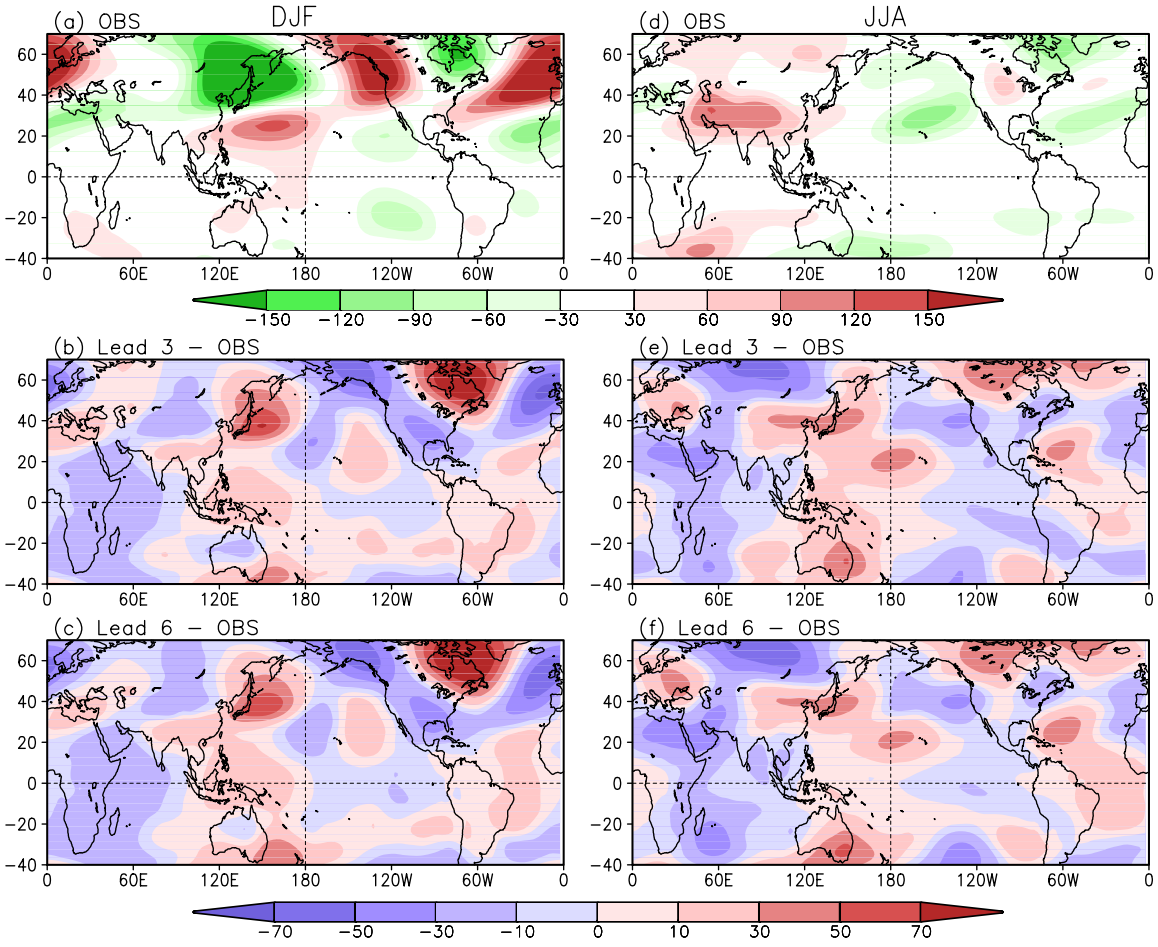

Fig. 17. As in Fig.15 but for 200hPa geopotential height. Unit is meters.

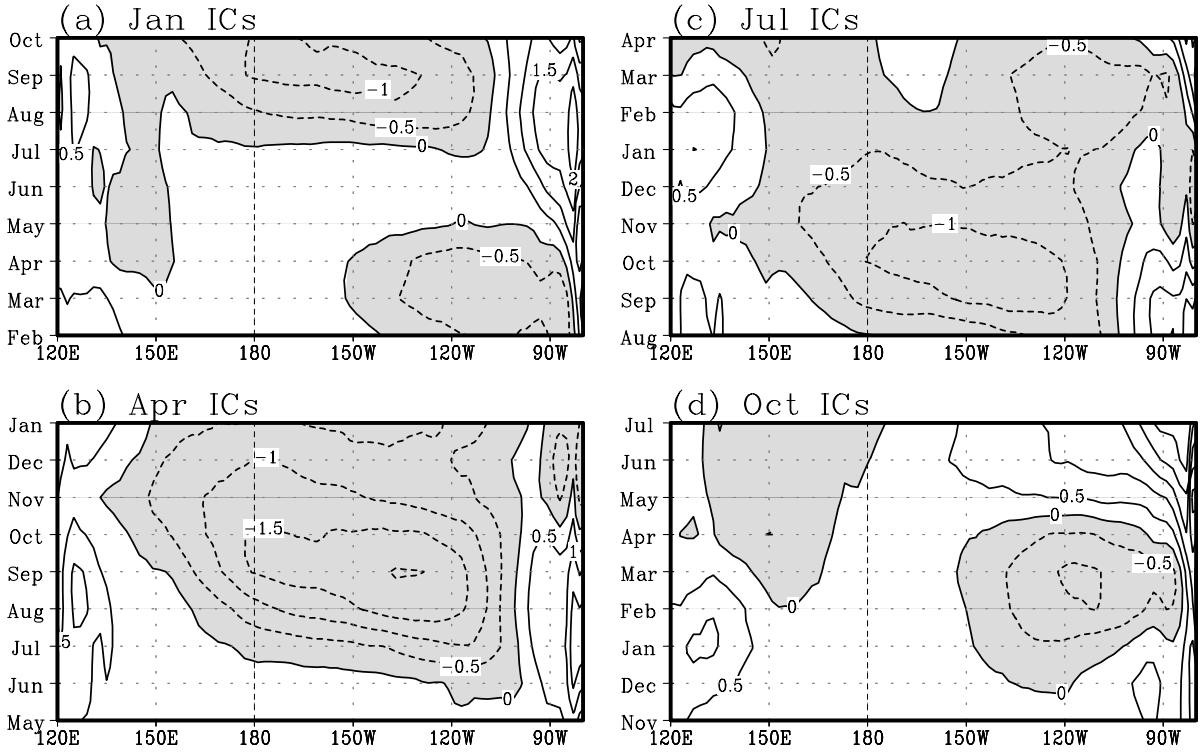

Fig. 18. Climate drift (Bias) of 2°S-2°N average SSTs in the Pacific for forecast from initial conditions of (a) January, (b) April, (c) July, and (d) October. Contours are drawn at 0.5 K interval. Negative values are shaded.

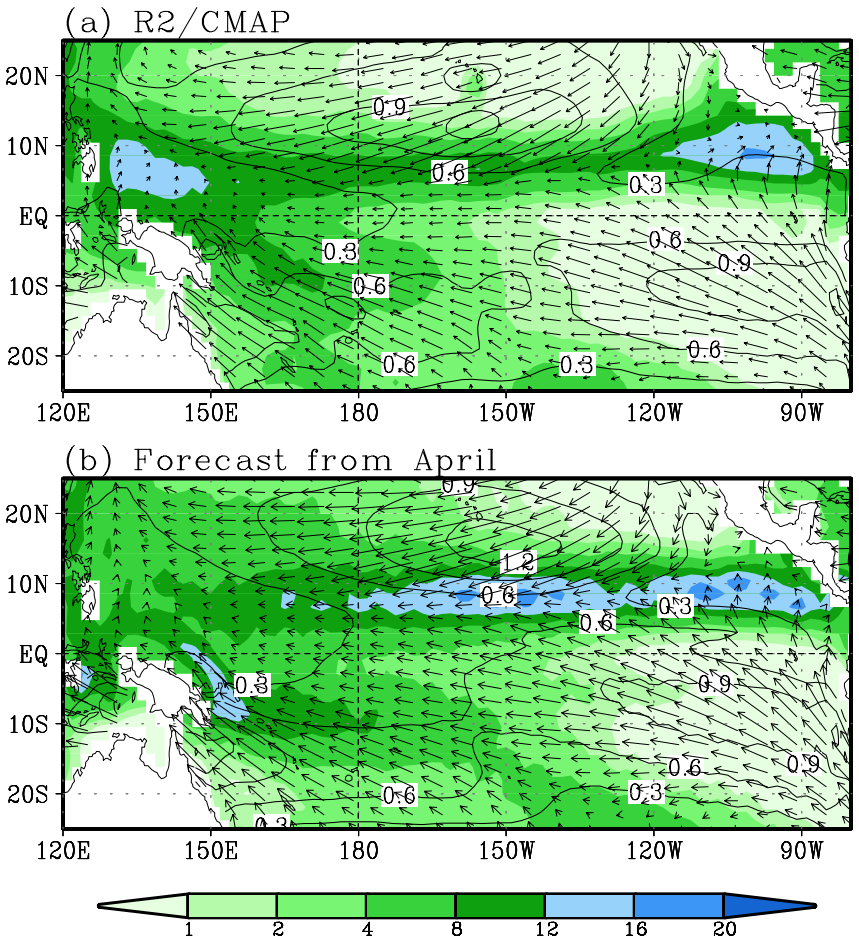

Fig. 19. Precipitation rate (color shadings) and surface momentum flux (vectors) of June from (a) R2/CMAP, and (b) forecast from April initial condition. Contours are the amplitude of surface momentum flux (0.1 N m^{-2}). Precipitation rate is shaded at 1, 2, 4, 8, 16, and 20 mm day^{-1}.

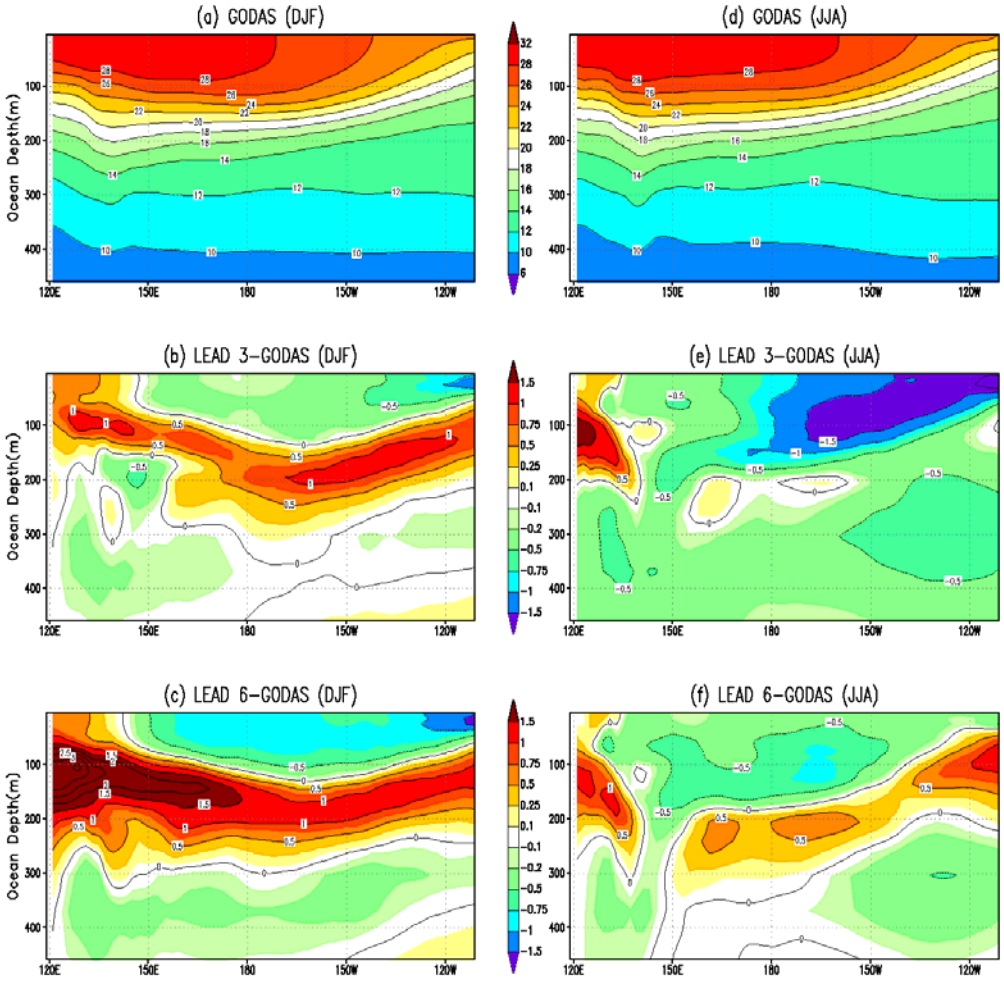

Fig. 20: The climatology of GODAS subsurface temperature in a depth-longitude cross section along the Equator in the Pacific and mean difference between the forecasts and GODAS in degrees Celsius. The figures on the left are for boreal winter (DJF), while the figures on the right are for boreal summer (JJA). The top panels show the climatology of subsurface temperature from GODAS. Note that a different scale is used for the color bar in the top panel.

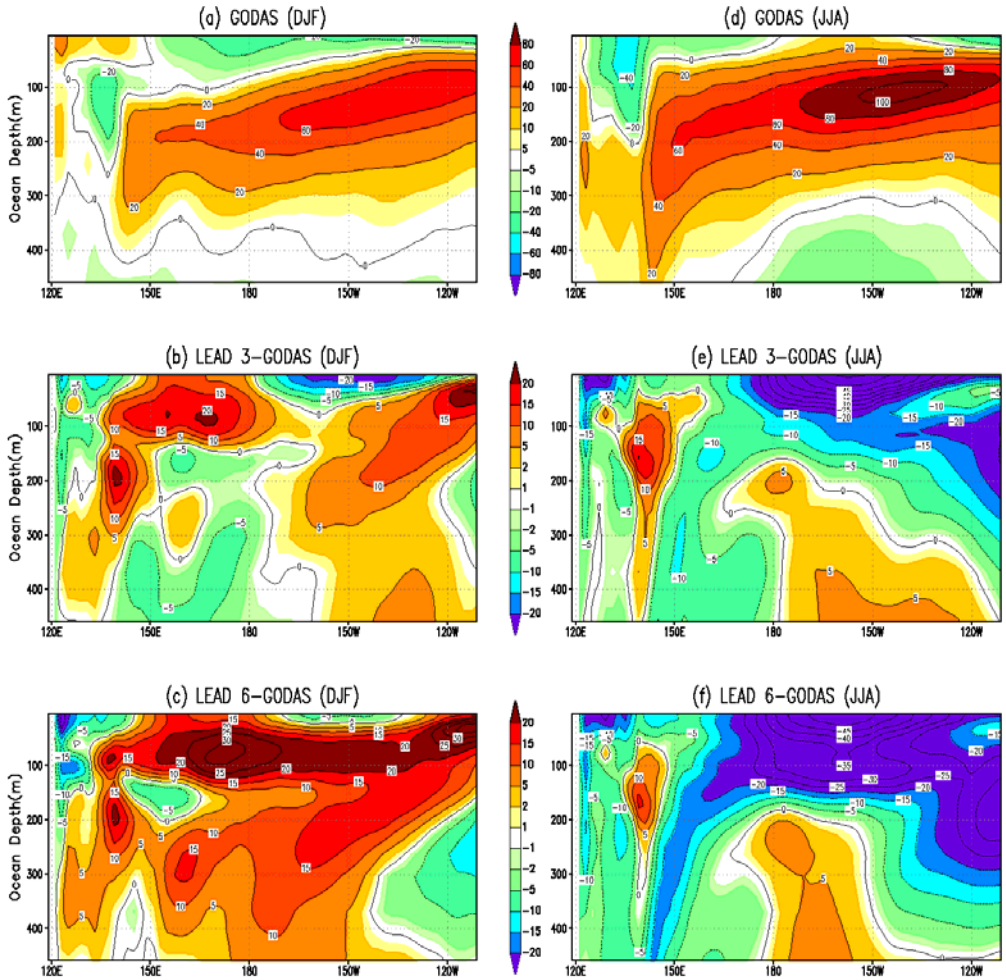

Fig. 21: As in Fig. 20 but now for zonal velocity in cm s^{-1}.

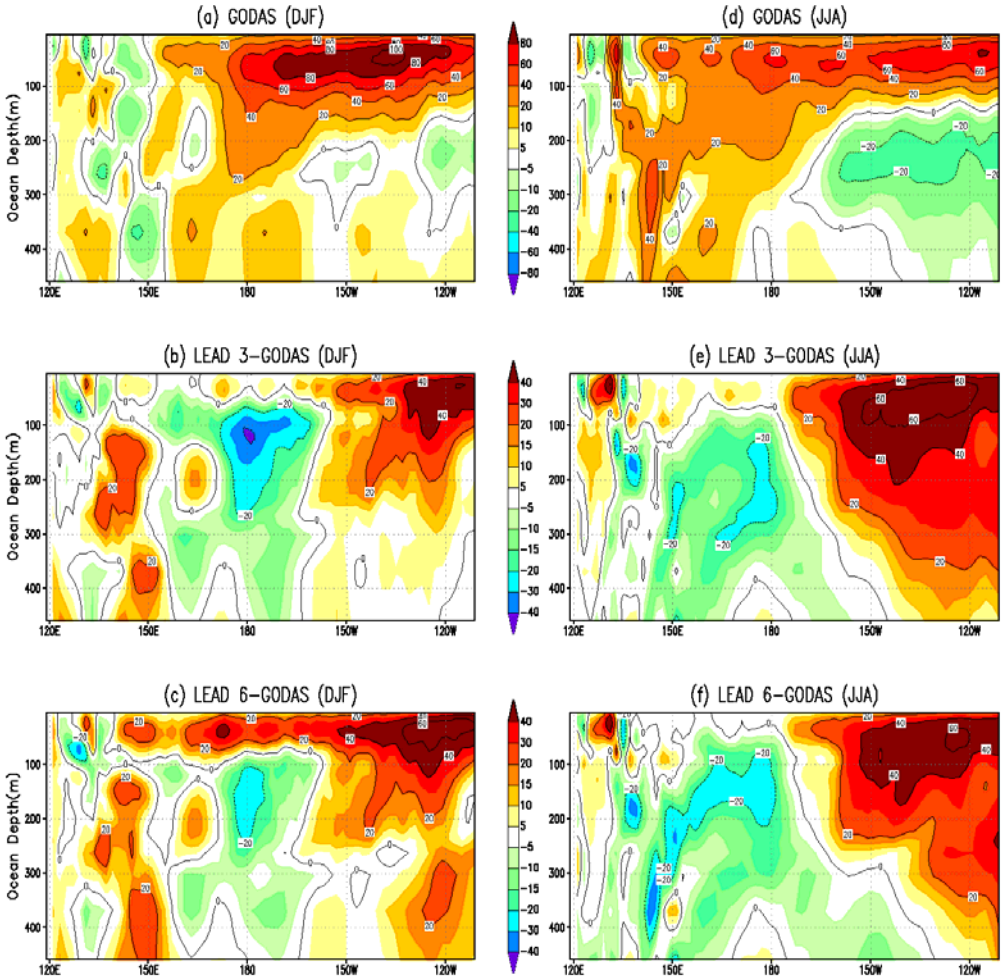

Fig. 22: As in Fig. 20, but now for vertical velocity in mm hour^{-1} .

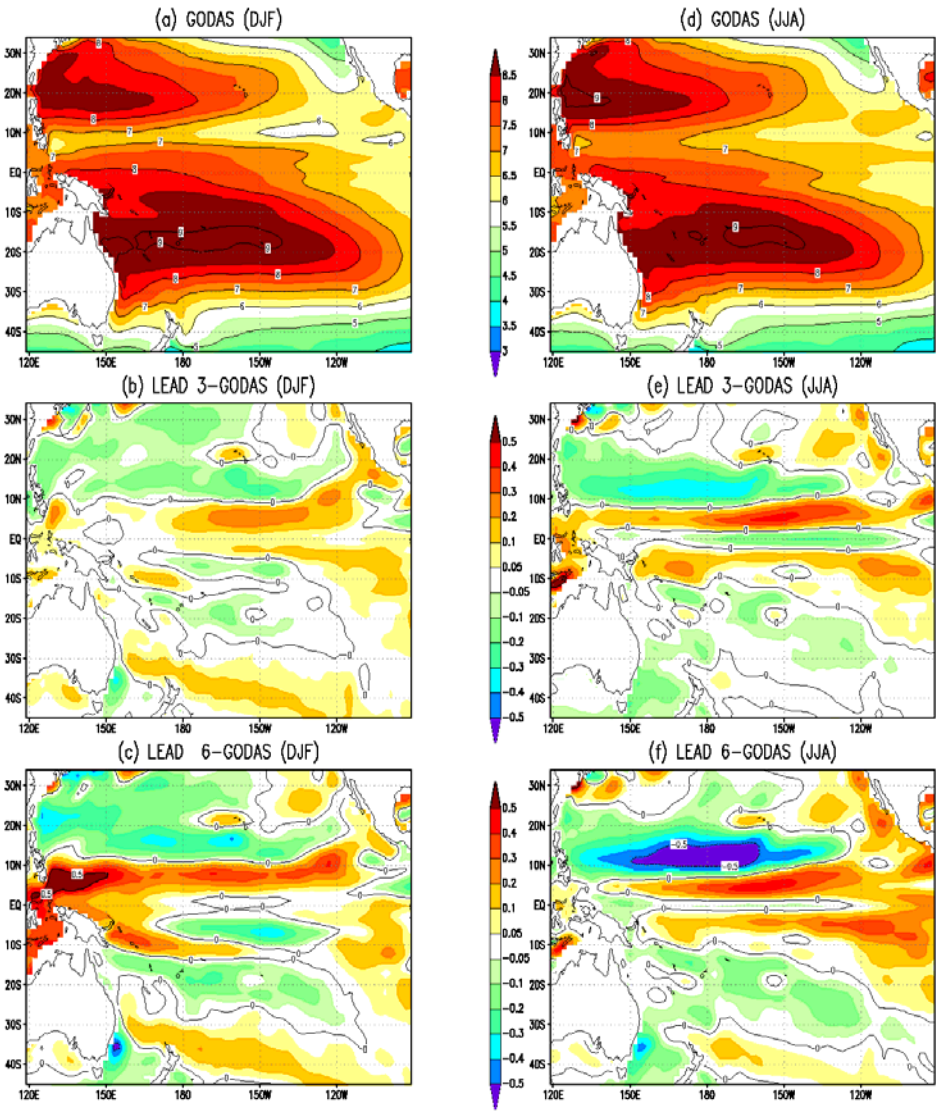

Fig. 23: As in Fig. 20, but now a latitudinal/longitudinal representation for the upper ocean heat content in 10^7 J m^{-2}.

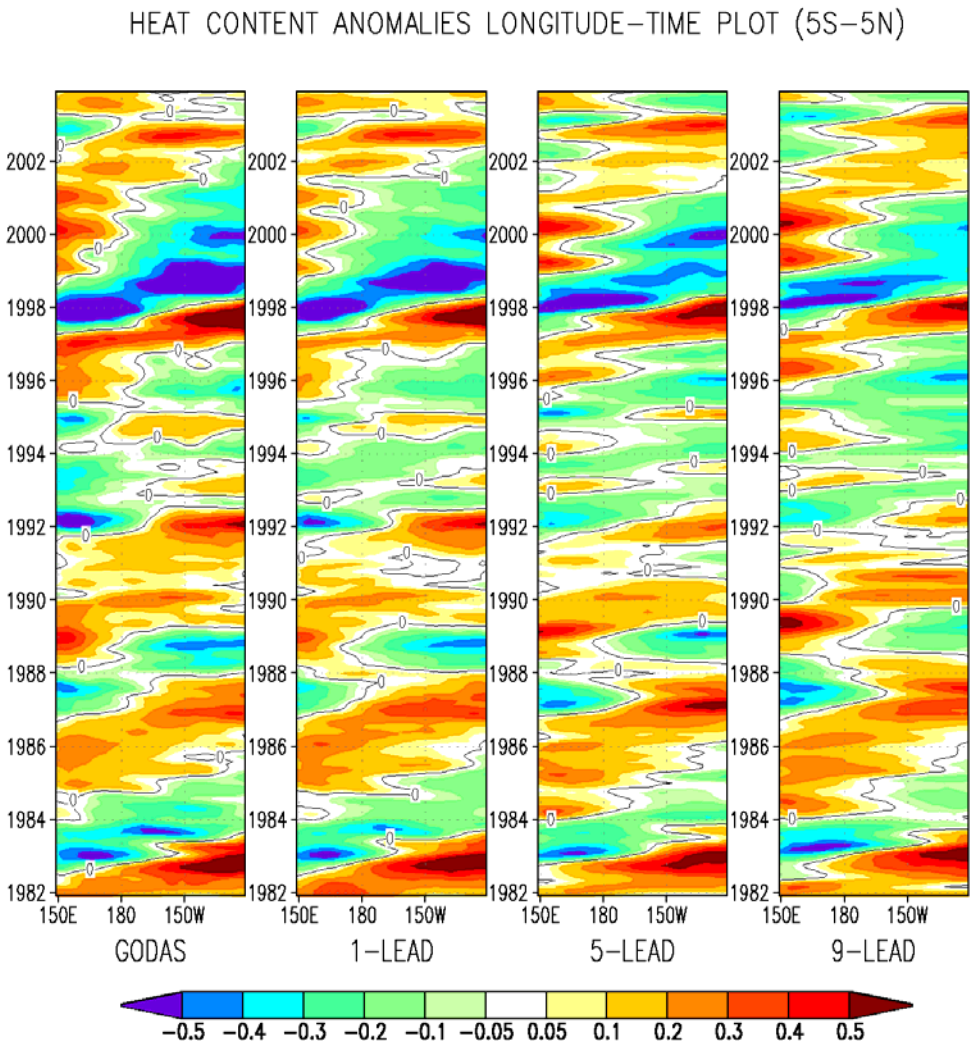

Fig. 24: Longitude-time plots of heat content anomalies along the equator in the Pacific from GODAS and CFS retrospective predictions. The climatology was computed for the period: 1982-2003. Unit is 10^7 J m^{-2}.

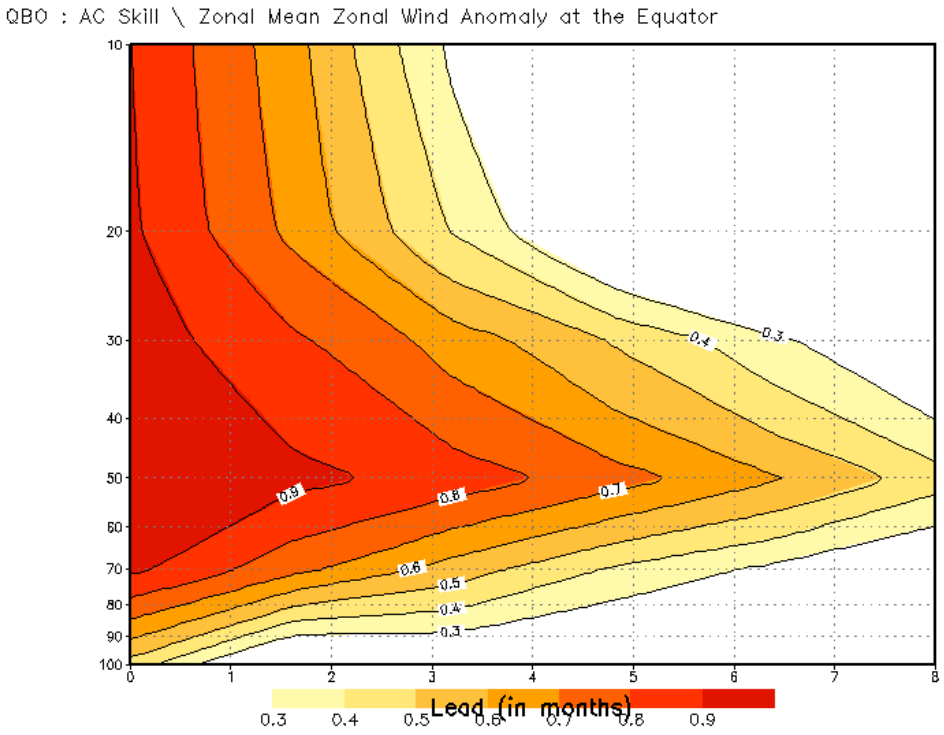

Fig. 25: Anomaly correlation of Zonal mean zonal wind anomaly at the equator as a function of pressure level (above 100 hPa) versus forecast lead time (in months).